



## PAPER

## Decoding spoken English from intracortical electrode arrays in dorsal precentral gyrus

RECEIVED  
30 June 2020REVISED  
11 September 2020ACCEPTED FOR PUBLICATION  
9 October 2020PUBLISHED  
11 November 2020Guy H Wilson<sup>1,12,13</sup> , Sergey D Stavisky<sup>2,3,4,12,13</sup> , Francis R Willett<sup>2,4,5</sup> , Donald T Avansino<sup>2</sup> ,  
Jessica N Kelemen<sup>6</sup> , Leigh R Hochberg<sup>6,7,8,11</sup> , Jaimie M Henderson<sup>2,3,14</sup> , Shaul Druckmann<sup>3,9,14</sup>   
and Krishna V Shenoy<sup>3,4,5,9,10,14</sup> 

- <sup>1</sup> Neurosciences Graduate Program, Stanford University, Stanford, CA, United States of America
- <sup>2</sup> Department of Neurosurgery, Stanford University, Stanford, CA, United States of America
- <sup>3</sup> Wu Tsai Neurosciences Institute and Bio-X Institute, Stanford University, Stanford, CA, United States of America
- <sup>4</sup> Department of Electrical Engineering, Stanford University, Stanford, CA, United States of America
- <sup>5</sup> Howard Hughes Medical Institute at Stanford University, Stanford, CA, United States of America
- <sup>6</sup> Department of Neurology, Harvard Medical School, Boston, MA, United States of America
- <sup>7</sup> Center for Neurotechnology and Neurorecovery, Dept. of Neurology, Massachusetts General Hospital, Boston, MA, United States of America
- <sup>8</sup> VA RR&D Center for Neurorestoration and Neurotechnology, Rehabilitation R&D Service, Providence VA Medical Center, Providence, RI, United States of America
- <sup>9</sup> Department of Neurobiology, Stanford University, Stanford, CA, United States of America
- <sup>10</sup> Department of Bioengineering, Stanford University, Stanford, CA, United States of America
- <sup>11</sup> Carney Institute for Brain Science and School of Engineering, Brown University, Providence, RI, United States of America

E-mail: [ghwilson@stanford.edu](mailto:ghwilson@stanford.edu) and [sergey.stavisky@stanford.edu](mailto:sergey.stavisky@stanford.edu)**Keywords:** speech decoding, intracortical, BCI, precentral gyrus, motor cortex, humanSupplementary material for this article is available [online](#)**Abstract**

*Objective.* To evaluate the potential of intracortical electrode array signals for brain-computer interfaces (BCIs) to restore lost speech, we measured the performance of decoders trained to discriminate a comprehensive basis set of 39 English phonemes and to synthesize speech sounds via a neural pattern matching method. We decoded neural correlates of spoken-out-loud words in the ‘hand knob’ area of precentral gyrus, a step toward the eventual goal of decoding attempted speech from ventral speech areas in patients who are unable to speak. *Approach.* Neural and audio data were recorded while two BrainGate2 pilot clinical trial participants, each with two chronically-implanted 96-electrode arrays, spoke 420 different words that broadly sampled English phonemes. Phoneme onsets were identified from audio recordings, and their identities were then classified from neural features consisting of each electrode’s binned action potential counts or high-frequency local field potential power. Speech synthesis was performed using the ‘Brain-to-Speech’ pattern matching method. We also examined two potential confounds specific to decoding overt speech: acoustic contamination of neural signals and systematic differences in labeling different phonemes’ onset times. *Main results.* A linear decoder achieved up to 29.3% classification accuracy (chance = 6%) across 39 phonemes, while an RNN classifier achieved 33.9% accuracy. Parameter sweeps indicated that performance did not saturate when adding more electrodes or more training data, and that accuracy improved when utilizing time-varying structure in the data. Microphonic contamination and phoneme onset differences modestly increased decoding accuracy, but could be mitigated by acoustic artifact subtraction and using a neural speech onset marker, respectively. Speech synthesis achieved  $r = 0.523$  correlation between true and reconstructed audio. *Significance.* The ability to decode speech using intracortical electrode array signals from a nontraditional speech area suggests that placing electrode arrays in ventral speech areas is a promising direction for speech BCIs.

<sup>12</sup> Authors to whom any correspondence should be addressed.<sup>13</sup> These authors are co-first authors.<sup>14</sup> These authors are co-last authors.

## 1. Introduction

Neurological disorders such as stroke and amyotrophic lateral sclerosis (ALS) take away the ability to speak from millions worldwide (Coppens 2016). In the case of ALS, loss of speech is often considered the worst aspect of disease progression, necessitating augmentative communication within 1–2 years of symptom onset (Makkonen *et al* 2018). Noninvasive assistive technologies such as sip-and-puff interfaces and eye tracking have helped re-establish communication, but suffer from low information transfer rates and limited expressivity (Tai *et al* 2008, Fager *et al* 2019). In contrast, speech is amongst the most intuitive and fastest means of communication, with conversational speech conveying roughly 150 words per minute (Chang and Anumanchipalli 2020). Brain-computer interfaces (BCIs) are an emerging technology through which a person's movement intentions are read out from their neural signals (Slutzky 2019, Tam *et al* 2019). A high-performance speech BCI that could accurately identify what people with speech loss want to say would therefore substantially improve patients' quality of life.

To gain direct access to the relevant neural signals, ongoing efforts to build speech BCIs, reviewed in (Chakrabarti *et al* 2015, Herff and Schultz 2016, Martin *et al* 2018, Rabbani *et al* 2019), have often used invasive electrocorticography (ECoG) measurements, in which electrode disks distributed across the cortical surface sample the aggregate activity of many tens of thousands of neurons under each recording site. This approach has been used in discrete classification of small speech building blocks such as phonemes, syllables, words, and sound snippets (Kellis *et al* 2010, Mugler *et al* 2014, Martin *et al* 2014, Bouchard and Chang 2014, Herff *et al* 2015, 2019, Salari *et al* 2018, Ramsey *et al* 2018). Recent work has also used neural networks to learn nonlinear mappings that transform neural signals into a variety of outputs such as acoustic speech features (Akbari *et al* 2019, Angrick *et al* 2019), including by way of intermediate articulatory kinematics (Anumanchipalli *et al* 2019), discrete targets such as phonemes or syllables (Livezey *et al* 2019), and entire phrases and sentences (Moses *et al* 2019, Makin *et al* 2020).

While the most advanced speech BCIs to date are ECoG-based, other recording modalities are also being investigated. These include non-surgical methods such as electroencephalography (Nguyen *et al* 2018) and magnetoencephalography (Dash *et al* 2020), stereotactic electroencephalography to access field potentials from deeper brain structures (Herff *et al* 2020), and intracortical electrodes capable of recording neuronal spiking activity (Guenther *et al* 2009, Brumberg *et al* 2011). The intracortical approach, which can in principle sample from many distinct sources of information (individual neurons

or small groups of neurons), is particularly promising for providing the sufficiently high neural bandwidth necessary to restore conversational speech. Intracortical BCIs that use multielectrode array signals to decode attempted arm and hand movements have demonstrated the highest performance to date for controlling computer cursors (Pandarinath *et al* 2017), high degree-of-freedom robotic arms (Collinger *et al* 2013), and the user's own arm muscles (Bolu *et al* 2017), with no prior user training (Brandman *et al* 2018). In contrast, intracortical BCIs for decoding speech are far less mature. Several studies have examined speech production using small numbers of intracortical recording sites in lateral temporal lobe (Creutzfeldt *et al* 1989, Tankus *et al* 2012), ventral motor cortex (Guenther *et al* 2009, Brumberg *et al* 2011), orbitofrontal cortex (Tankus *et al* 2012), and subthalamic nucleus (Lipski *et al* 2018, Tankus and Fried 2019). Ninety-six-electrode Utah arrays, of the type used in the aforementioned arm and hand BCIs, have been placed into superior temporal gyrus to decode heard speech in monkeys (Heelan *et al* 2019) and both heard and spoken speech in a person (Chan *et al* 2014). However, these previous studies did not use large numbers of electrodes to record from motor areas of cortex, which is the approach that has proved promising for restoring arm and hand function.

We are positioned to start to address this gap after having recently found speech-related activity in the dorsal 'hand/knob' area of precentral gyrus (Stavisky *et al* 2019, Willett *et al* 2020b), where a number of groups already place Utah arrays. These signals could be used to discriminate between a small number of syllables and words with high accuracy (Stavisky *et al* 2018, 2019, 2020). In the present study, we build on this discovery to further evaluate the potential of using intracortical signals from two Utah arrays to decode among 39 phonemes, which could be used as a comprehensive basis set in a speech BCI, and to reconstruct speech sounds using the Brain-to-Speech pattern matching technique of (Herff *et al* 2019). Importantly, we recorded from the dorsal precentral gyrus of two people with tetraplegia who already had arrays placed as part of their participation in the BrainGate2 clinical trial, which has the primary goal of evaluating the safety of these intracortical BCI devices. We recognize and wish to highlight that this cortical area, which has a well-established role in volitional arm and hand movements (Hochberg *et al* 2006, 2012, Collinger *et al* 2013, Wodlinger *et al* 2015, Bouton *et al* 2016, Pandarinath *et al* 2017, Ajiboye *et al* 2017, Downey *et al* 2018b, Rastogi *et al* 2020) and modulates to a lesser extent during movements of other body parts (Stavisky *et al* 2019, Willett *et al* 2020b), is likely sub-optimal for decoding speech. Nonetheless, this research context also presents a rare opportunity to evaluate the feasibility of decoding speech production from

many simultaneously recorded intracortical signals, using ground truth data from people who can still speak, without additional risk. Our guiding motivation is that the results of this investigation should be viewed as a lower bound proof-of-concept on the intracortical performance that ought to be possible, and that higher performance will be possible with arrays specifically placed in ventral speech cortex where previous ECoG studies have shown strong speech production-related modulation (Kellis *et al* 2010, Takai *et al* 2010, Bouchard *et al* 2013, Mugler *et al* 2018, Chartier *et al* 2018, Herff *et al* 2019).

We recorded neural signals as the participants spoke out loud a set of 420 different short words. This set included most of the same spoken words as previous ECoG studies (Mugler *et al* 2014, Herff *et al* 2019), which allowed us to make a well-matched comparison between decoding Utah array signals and these previous ECoG results. We first examined whether neural firing rates changed when the participant spoke just one or a handful of phonemes ('sparse tuning'), or across speaking many phonemes ('broad tuning'). This measurement is important for assessing the viability of intracortical speech BCIs, which in the near-term are likely to be restricted to hundreds (not thousands) of electrodes within a relatively localized area of cortex. We found that activity recorded on these electrodes had broad tuning; this encoding scheme makes it more likely that signals related to producing all the phonemes will be observable from a limited number of electrodes, and also has previously been shown to be more robust and decodable (Abbott and Dayan 1999). Next, we trained both conventional and deep learning classifiers to predict which of 39 phonemes was being spoken, using the available neural signals. We found that decoding performance was better using high-frequency local field potentials (HLFP) rather than threshold crossing spikes (TCs) (i.e. action potentials from one or potentially several neurons near an electrode tip detected when the measured voltage drops below a set threshold), and was competitive with previous ECoG decoding performance (Mugler *et al* 2014). Encouragingly, subsampling the data used for decoder training indicated that speech BCI performance is likely to improve as more training data and electrode recording sites become available. We also evaluated reconstructing continuous speech from these neural data by combining audio snippets corresponding to the closest matching neural window in a training data set, and again observed comparable performance to reported ECoG speech synthesis using the same technique (Herff *et al* 2019).

While there are many advantages to using overt speaking data to establish proof-of-feasibility for a speech BCI, this widely used model (Suppes *et al* 1997, Kellis *et al* 2010, Bouchard and Chang 2014, Pailla *et al* 2016, Mugler *et al* 2014, Herff *et al* 2015, Ramsey *et al* 2018, Salari *et al* 2018, Angrick

*et al* 2019, Herff *et al* 2019, Moses *et al* 2019, Anumanchipalli *et al* 2019, Livezey *et al* 2019; Makin *et al* 2020) also introduces potential confounds. Here we investigated two potential limitations which have received little prior attention. The first is that using the recorded audio signal to detect voice onset may introduce systematic onset time biases across phonemes due to differences between when voice sounds become detectable versus when the speech articulators are being moved. This in turn can exaggerate neural differences between phonemes by artificially shifting what are actually condition-invariant neural signal components. The second confound, which was recently raised by Roussel and colleagues (Roussel *et al* 2020), is that mechanical vibrations due to speaking might cause microphonic artifacts in the neural recordings. Our analyses suggest that while these confounds most likely do inflate speech decoding performance, their effects are not large. Furthermore, we introduce analysis methods that can be applied to neural data collected during overt speech to mitigate these confounds.

## 2. Methods

### 2.1. Participants

Research sessions were conducted with volunteer participants enrolled in the BrainGate2 pilot clinical trial (ClinicalTrials.gov Identifier: NCT00912041). The trial is approved by the U.S. Food and Drug Administration under an Investigational Device Exemption (Caution: Investigational device. Limited by Federal law to investigational use) and the Institutional Review Boards of Stanford University Medical Center (protocol #20 804), Brown University (#0809992560), and Partners HealthCare/Massachusetts General Hospital (#2011P001036). The BrainGate2 trial's purpose is to collect preliminary safety information and demonstrate feasibility that an intracortical BCI can be used by people with tetraplegia for communication and control of external devices; the present manuscript results from analysis and decoding of neural activity recorded during the participants' engagement in research that is enabled by the clinical trial but does not report clinical trial outcomes.

Participant T5 is a right-handed man who was 65 years old at the time of the study. He was diagnosed with C4 AIS-C spinal cord injury 11 years prior to this study. T5 is able to speak and move his head, and has residual movement of his left bicep as well as trace movement in most muscle groups. Participant T11 is an ambidextrous man who was 35 years old at the time of the study. He was diagnosed with C4 AIS-B spinal cord injury 11 years prior to this study. T11 is able to speak and move his head. He has some residual movement in both arms. Both participants gave informed consent for this research and associated publications.

## 2.2. Many words task

The participants performed a simple visually prompted speaking task. On each trial they spoke one of 420 unique words that widely sample American English phonemes. The words used are an expanded set of the Modified Rhyme Test (House *et al* 1963, Mines *et al* 1978) and were previously used in several other studies (Mugler *et al* 2018, Herff *et al* 2019, Angrick *et al* 2019). They include most, but not all, of the words used in Mugler and colleagues' study (Mugler *et al* 2014). These words were visually prompted (and subsequently spoken) one at a time. The participant was seated while fixating on a colored square centered on a computer screen in front of him. A trial started with an instruction period lasting 1.2 to 1.8 s, in which the central square was red, and white text above it instructed the word (e.g. 'Prepare: "Word"; see figure 1(B)). The participant subsequently spoke the prompted word out loud following a go cue, which consisted of the square turning green, the text changing to 'Go,' and an audible beep. The next trial began ~2.5 s later. Trials were presented in continuous blocks separated by short breaks, with the entire 420 word corpus divided across four blocks. Participant T5 performed three repetitions of each word (12 total blocks). Participant T11 performed 11 total blocks resulting in two to three repetitions of each word. Data from participant T5 were previously analyzed in (Stavisky *et al* 2019), which examined the phonemic structure of trial-averaged, phoneme-aligned firing rates. The T11 data have not previously been reported.

Phoneme classes with at least 30 repetitions in the T5 dataset were included in the phoneme-specific analyses (e.g. classification), resulting in a set of 39 different phonemes. One phoneme in the T11 dataset (/ɔi/) had fewer repetitions (26) but was nonetheless included for consistency across the two participants. Two phonemes which otherwise would have had too few repetitions for inclusion were consolidated with a very similar phoneme with more repetitions: /ɔ/ (14 T5 utterances, 14 T11 utterances) was grouped with /ʌ/ (115 T5 utterances, 96 T11 utterances), and /ɜ:/ (18 T5 utterances, 18 T11 utterances) was grouped with /ɜ:/ (30 T5 utterances, 29 T11 utterances).

In the phoneme classification analyses shown in supplementary figure 2 available online at [stacks.iop.org/JNE/17/066007/mmedia](https://stacks.iop.org/JNE/17/066007/mmedia), we sought to match, as best we could, a set of words for comparing phoneme decoding with that of a previous ECoG phoneme decoding study by Mugler and colleagues (Mugler *et al* 2014). Our word set already had 256 of the 320 words of that study; these we included in our 'matched' data subset. To fill out the remaining 64 words, we picked similar words from the 190 additional words in our overall dataset. Our substituted words have the same total number of phonemes as the words we were missing from the Mugler and colleagues report (Mugler *et al* 2014), and typically

differed in only one or two phonemes. Examples of these substitutions are 'bill' (bil) → 'bell' (beɪ), 'late' (leɪt) → 'loot' (lut), 'mass' (mæs) → 'mouse' (maʊs), 'ray' (rei) → 'reach' (ri:tʃ), 'tip' (tɪp) → 'type' (taɪp).

## 2.3. Intracortical electrode array recording

Participants T5 and T11 had two 96-electrode Utah arrays (Blackrock Microsystems Inc., Salt Lake City, USA) neurosurgically placed in the 'hand knob' area of their left dorsal motor cortex 29 months (T5) and 3 months (T11) prior to this study (figure 1(A)).

Neural signals were acquired with a NeuroPort™ system (Blackrock Microsystems Inc.), analog filtered from 0.3 Hz to 7500 Hz, and digitized at 30 000 Hz at 16 bits/sample.

## 2.4. Neural signals

We common average referenced each electrode by subtracting the mean voltage across all other electrodes from its time series at each timepoint. Action potentials (spikes) were detected based on when voltage values became more negative than a threshold set at  $-3.5 \times$  root mean square of that electrode's voltage. We did not spike sort these TCs, which may capture action potentials from one or more neurons near the electrode tip, since here we were interested in decoding the neural state rather than characterizing the properties of putative single neurons (Collinger *et al* 2013, Oby *et al* 2016, Bolu *et al* 2017, Pandarinath *et al* 2017, Brandman *et al* 2018, Even-Chen *et al* 2018, Trautmann *et al* 2019). The voltage time series were also bandpass-filtered using a 3rd order bandpass Butterworth causal filter from 125 to 5000 Hz to extract HLF signals, which have been previously shown to contain useful motor-related information (Pandarinath *et al* 2017, Stavisky *et al* 2018, 2019, Nason *et al* 2020).

## 2.5. Audio recording

Audio recordings were made using a microphone (Shure SM-58), pre-amplified by ~60 dB (ART Tube MP Studio microphone pre-amplifier), and digitized at 30 000 Hz by the NeuroPort system via an analog input port.

Phoneme identities and onset times were manually labeled using the Praat software package (Boersma 2001). The spoken words contained between two and six phonemes with a majority being three phonemes long (supplementary figure 1(A)). Supplementary figure 1(B)–(C) shows the distribution of phoneme audio durations. Although the same word prompt set was used for both participants, participant T5 completed one additional block of the many words task, and both participants occasionally misspoke or chose to speak different words that

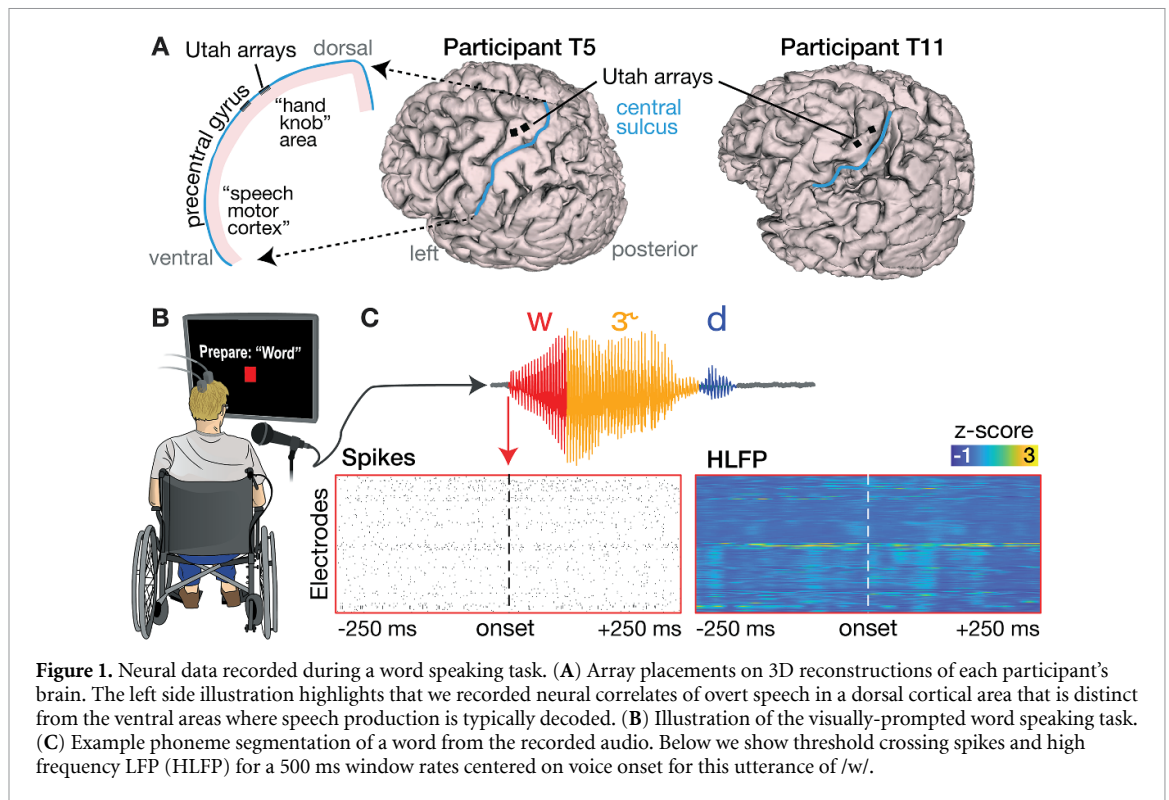


**Figure 1.** Neural data recorded during a word speaking task. (A) Array placements on 3D reconstructions of each participant's brain. The left side illustration highlights that we recorded neural correlates of overt speech in a dorsal cortical area that is distinct from the ventral areas where speech production is typically decoded. (B) Illustration of the visually-prompted word speaking task. (C) Example phoneme segmentation of a word from the recorded audio. Below we show threshold crossing spikes and high frequency LFP (HLFP) for a 500 ms window rates centered on voice onset for this utterance of /w/.

are spelled the same way (e.g. 'tear'). Thus, the exact utterance count (T5: 3840, T11: 3467) and distribution of spoken phonemes differed between participants.

## 2.6. Neural feature extraction and classification models

HLFP activity was clipped at  $100 \times$  median activity for each electrode to lessen the impact of rare, large-amplitude electrical noise artifacts. Furthermore, one trial from each of the participants' datasets was removed due to a very large simultaneous noise artifact across all electrodes. HLFP and spike rasters were temporally smoothed using a moving average filter (20 milliseconds with 1 millisecond steps), resulting in time series of binned TCs firing rates and HLFP power. Electrodes were then visually inspected and those with baseline firing rate nonstationarities or visible noise were excluded from the neural analyses; this resulted in 158 and 179 included electrodes for T5 and T11, respectively.

We trained (1) a multi-class logistic regression model and (2) a recurrent neural network (RNN) to predict phoneme identity from neural features using the Scikit-learn and Tensorflow (version 1.15.0) libraries respectively (Pedregosa *et al* 2011, Abadi *et al* 2016). Both models were trained in a cross-validated classification setup using multiple bins of activity per electrode as described below.

Except where otherwise mentioned, we extracted a 500 millisecond window of neural activity centered around the onset of each phoneme. This specific value, while somewhat arbitrary, was chosen

to match a previous ECoG phoneme decoding study (Mugler *et al* 2014) and exceeds the typical duration of the participants' spoken phonemes (supplementary figure 1). Figures 3(E), (J) examines a wider range of neural activity analysis windows. For the logistic regression model, we averaged activity in this window within non-overlapping 50 millisecond bins (Mugler *et al* 2014) and z-score normalized their magnitudes to account for different electrodes' activity ranges. We then compressed the resulting feature set using principal components analysis (PCA, 75% variance retained). Z-score normalization mean and standard deviation (s.d.), and PCA coefficients were calculated from within each training fold and then applied to the test data.

For the RNN decoder analysis (see section 2.8: *RNN decoder*), we did not discard the 34 T5 electrodes as described above and instead used all 192 electrodes. Our reasoning was that even non-stationary or noisy electrodes could potentially be used by the RNN (Sussillo *et al* 2016). In practice, however, this made little difference: the RNN decoder with the same electrode exclusions as the linear decoder performed at 32.4% accuracy, compared to 33.9% without excluding any electrodes.

## 2.7. Logistic regression for phoneme classification

The logistic regression model was trained using the Scikit-learn library (Pedregosa *et al* 2011) in a leave-one-out cross-validation setup using default parameters except for the 'lbfgs' optimization setting and L2 regularization value ( $\lambda = 100$ ) to suppress overfitting. For multi-class classification, we used a

one-vs-rest scheme where a different model is trained for each class to discriminate it against all others. For a given phoneme, model predictions are pooled and the highest positive class likelihood across models is taken as the decoder estimate.

We used 20-fold cross-validation for generating the phoneme classifications shown in figures 4, 5(E)–(F). We used leave-one-out cross-validation for the phoneme classifications shown in figures 3(A), 3(F), 5(D) and supplementary figure 2. For all hyperparameter sweeps (figure 3), we used ten repetitions of a 10-fold cross-validation procedure. Training data duration sweeps were performed by taking fractions of the overall phoneme data and then, for each such fraction, calculating the mean training data audio duration across training folds. This approach ensured that audio length estimates were not inflated by overlapping phoneme windows in the same training fold (e.g. if two consecutive phonemes are included), which would be the case if we had simply multiplied the number of phonemes used by our 500 millisecond window. The ‘number of electrodes’ hyperparameter sweep was performed by randomly selecting a specific number of electrodes for both training and testing, and repeating this sampling 10 times for each number of electrodes.

To test for structure in the decoder’s misclassifications of T5’s neural data, we sorted our confusion matrix, where entry  $(i, j)$  corresponds to the percentage of times the  $i$ th phoneme in our decoding set is classified as the  $j$ th, by place of articulation (as in (Moses *et al* 2019, Stavisky *et al* 2019)) and measured the difference between within- and between-group confusions. We then built a null distribution of expected differences if there were no underlying structure correlated with place of articulation in these errors by generating random partitions of our phonemes (keeping the same group sizes) and re-measuring the test statistic 10 000 times from these permuted data.

## 2.8. RNN decoder

An RNN was trained to predict phoneme identities from 1000 ms neural data snippets from each electrode, each subdivided into fifty 20 ms bins. The RNN was built as a single layer of 512 bidirectional gated recurrent units (Cho *et al* 2014) implemented with the cuDNN library (Nvidia Corp., Santa Clara, USA). When training, the input data at each 20 ms time step was the 192-dimensional HLFP feature vector, while the supervised target output was a 39-dimensional ones-hot vector where the element corresponding to the phoneme associated with this data snippet was set to 1, and all other phonemes were set to 0 (supplementary figure 3(A)). The training cost function also included a L2 regularization term to penalize large network weights ( $\lambda = 1e-5$ ). During testing, for each phoneme utterance a new  $192 \times 50$  neural data matrix was input to the RNN, and a  $39 \times 50$  output matrix was read out, which consisted of the

RNN’s predicted likelihoods (logits) that the input data came from each of the 39 possible phonemes, for each bin. The most likely phoneme during the last bin was chosen as the RNN’s final prediction for that snippet (supplementary figure 3(B)). The RNN was trained and evaluated across 10 folds of the data, such that each spoken phoneme utterance appeared in the test set once.

Given the relative paucity of available Many Words Task speaking data compared to the data corpus sizes in typical machine learning applications, two additional training data augmentation methods were used to regularize the RNN and prevent it from overfitting on the training data. These were adapted from our group’s recent work using RNNs to decode the neural correlates of handwriting (Willett *et al* 2020b) and conform to lessons learned from a previous iBCI RNN decoding study (Sussillo *et al* 2016). First, white noise (s.d. = 0.1) was added to each time bin’s neural input feature vectors during training. Second, more slowly-varying artificial neural input feature drifts were added across the time bins of each snippet during training to make the RNN robust to potential nonstationarities in the neural data (Perge *et al* 2013, Jarosiewicz *et al* 2015, Downey *et al* 2018a). These drifts had two components: a constant offset vector applied separately to each utterance (s.d. = 0.6), and a random walk across bins (s.d. = 0.02).

The RNN was trained using the ‘Adam’ gradient descent optimization (Kingma and Jimmy 2017) with a mini-batch size of 128 utterances, with no burn in steps, for 20 000 mini-batches. The learning rate decreased linearly from 0.01 (first mini-batch) to 0 (last mini-batch).

In order to directly and fairly compare this RNN approach to the logistic regression described in the previous section, we also trained and evaluated a logistic regression model using the exact same input data (including the same specific ten cross-validation folds) as used for the RNN decoder evaluation.

## 2.9. Demixed PCA (dPCA)

We used dPCA (Kobak *et al* 2016) to decompose population activity into components reflecting variance that can be attributed to phoneme classes and time (‘phoneme-dependent’) or time only (phoneme-independent). Specifically, we took a 1500 ms window centered on voice onset and decomposed it into low-rank approximations that captured phoneme class-dependent and independent variance. Spike rasters were convolved with a symmetrical 25 ms s.d. Gaussian and then averaged within 10 ms, non-overlapping bins before applying dPCA.

To ensure that dPCs were not fitting to noise, we adopted the cross-validation procedure described in (Willett *et al* 2020b) to obtain 95% confidence intervals. We split our trials into ten separate folds to cross-validate dPC decompositions, thus avoiding

overfitting to dataset noise. For each fold, all other folds are used to identify a dPCA decomposition. We then projected the held-out trials onto the identified dPCs. Geometrically, dPCA finds a linear subspace of a marginalized feature space where the axes correspond to a reconstruction error-minimizing subspace. Flipping the orientation of these vectors will preserve this subspace and hence also satisfy the optimization, but can confuse visualizations and comparisons across dPCA application instances. To avoid this issue and facilitate dPC comparisons across folds, we multiplied our components by  $-1$  when this would result in a smaller angle between the  $k$ th principal components in a given marginalization.

We used the largest phoneme-independent neural component, which we refer to as the 1st component of the condition-invariant signal (CIS<sub>1</sub>) as in (Kaufman *et al* 2016), to determine when phoneme production started from the neural data. This is in contrast to using acoustic data (figure 4). To do so, we trial averaged the neural activity for a given phoneme within each cross-validation fold and projected the resulting electrodes by time matrix onto the CIS<sub>1</sub> neural dimension. This yields 10 CIS<sub>1</sub> peak estimates (for 10 folds). The average CIS<sub>1</sub> time course across these ten folds was used to determine each phoneme's CIS<sub>1</sub> peak (the time of maximum CIS<sub>1</sub> value), which determined that phoneme's neurally-derived onset. In practice, this approach is similar to simply aligning to the peak of each phoneme's trial-averaged mean population firing rate (the Pearson correlation between CIS<sub>1</sub> peaks and mean rate peaks was  $r = 0.669$ ,  $p = 0.002$ ), but is more principled since dPCA explicitly searches for a condition-invariant projection of the data.

### 2.10. Quantifying acoustic artifact and linear regression reference (LRR) decontamination

To compare spectral content between recorded audio and electrodes (figures 5(A)–(B)), we convolved the voltage time series of each electrode and also the audio channel with a 200 ms Hamming window and then computed the power spectral density (PSD) in non-overlapping bins using a short-time Fourier transform (as in Roussel *et al* 2020). We isolated 'voicing epochs' in which to compare audio and neural power time series by sub-selecting time points with summed audio power (across all frequencies) in the top  $\sim 10\%$  of values across all audio data. For spectrogram visualizations in figure 5(A), sliding time windows overlap by 90%.

The LRR procedure (Young *et al* 2018) to remove putative acoustic contamination from each electrodes' signal began with fitting linear regression models that predicted each electrode's voltage (bandpass-filtered in the 125–5000 Hz range using a third-order Butterworth filter) at a given time sample from every other electrode's voltage at that time sample. Regression weights were fit separately within

each block in order to increase reliability if there were across-block changes in the acoustic contamination (if, for example, the participant shifted posture). These linear models were fit using the scikit-learn library's (Pedregosa *et al* 2011) *SGDRegressor* class with default parameters save for regularization strength ( $\alpha = 400$ ), early stopping, and initial learning rate ( $\eta = 0.0000004$ ). Hyperparameter values were identified based upon manual tuning. Regressions were fit using voltage activity occurring during voicing epochs. These timepoints were identified by extracting the acoustic envelope using a Hilbert transform and then thresholding based upon a manually identified threshold.

### 2.11. Tuning fork control for microphonic pickup

We performed this control experiment during a separate research session with participant T5, 12 months after his primary Many Words Task session. The participant was seated in his chair, facing the microphone, and connected to the full recording system in the same way as during the primary data collection. The participant was asked to sit quietly, relax, and avoid moving while a researcher activated a tuning fork (by striking it with a mallet) and then held it in the air just in front of the participant's head. The researcher then touched the tuning fork's stem against T5's head, then against each Blackrock cable pre-amplifier, and finally against each of the hanging cables itself. The participant reported that he could hear and/or feel the vibrations in all conditions but that they did not cause any discomfort.

We identified 7 s audio and neural snippets corresponding to when the tuning fork was activated and applied to the head/pre-amplifier/cable. Power spectrograms were calculated for these snippets' raw voltage signals (sampled at 30 000 Hz with no additional filters applied except for the analog filters of the Blackrock Neural Signal Processor) using a short time Fourier transform (50 ms windows, 1 ms sliding window, 7.3 Hz resolution).

### 2.12. Speech synthesis via unit selection

Speech audio was reconstructed offline using the 'Brain-to-Speech' synthesis method recently developed by Herff and colleagues (Herff *et al* 2019). To facilitate comparison with this previous ECoG study, we closely followed their methods and used the same set of spoken word prompts (although the exact set of utterances was not identical due to different trial counts and occasional missed trials or word substitutions). In overview, this unit selection-based approach (Hunt and Black 1996) consists of creating a training library of speech units (brief snippets of audio) with corresponding neural feature vectors. Then, for 'new' neural data (here, held out test data), the closest matching neural data in the training library is identified. The audio snippet corresponding to this best matching neural data is selected for the

speech reconstruction. This procedure advances step by step, selecting and concatenating together these best neurally-matching audio snippets until speech sound has been synthesized for the entire test epoch (here, one word and the silence immediately preceding and/or following it). The resulting performance is assessed by comparing the synthesized speech audio with the true spoken audio.

The T5 Many Words Task data were divided into ten folds for cross-validation, and the overall procedure was repeated such that each fold was used once for testing against a decoder trained on the remaining 90% of the data. An audio snippet unit was constructed at every 10 ms step of the recorded speech data. Each audio snippet was a 150 ms duration Hanning window, which facilitates smooth transitions when concatenating partially overlapping units.

For each audio snippet unit, a corresponding neural feature vector was generated as follows. HLFP power was calculated, clipped at  $100 \times$  median activity, and z-scored as described earlier. From each electrode, a 650 ms window (centered on the center of the audio snippet) of these neural data were divided into 13 non-overlapping 50 ms bins and time-averaged within each bin. The choice of 13 bins differs slightly from (Herff *et al* 2019), who used eleven 50 ms bins (450 ms total window); we opted for 650 ms based on the phoneme decoding parameter sweeps in figure 3(E). This yielded a  $158 \text{ electrodes} \times 13 \text{ bins} = 2054$ -dimensional neural vector for each audio snippet. Given the high dimensionality of these neural features relative to the amount of training data ( $\sim 138\,000$  training samples per fold), we reduced the neural feature dimensionality (a form of regularization to reduce overfitting) using PCA. As in (Herff *et al* 2019), we kept as many principal components as necessary to explain at least 70% of the total neural variance, which for these data required 25 principal components. The training and test folds were constructed such that no test fold words were present in the training fold. Furthermore, PCA coefficients and neural feature means, medians, and standard deviations (for clipping and z-scoring) were computed only from the training fold, and then applied to the test fold.

For each 10 ms step of the test data, speech synthesis proceeded as follows. The 25-dimensional neural feature vector corresponding to this step,  $\mathbf{x}_t$ , was compared to all  $N$  training data neural features  $\mathbf{x}_{i=1, \dots, N}$  using cosine similarity, and then the closest matching training sample was selected:

$$i = \arg \max_i \{ (\mathbf{x}_t \cdot \mathbf{x}_i) / (\|\mathbf{x}_t\| \|\mathbf{x}_i\|) \}$$

The 150 ms audio snippet corresponding to training index  $i$  was then added to the synthesized speech, overlapping with 140 ms of the existing synthesized audio. This procedure was repeated for the entire test word. As in (Herff *et al* 2019), we did not use any

concatenation cost when selecting the best matching audio unit (i.e. we did not apply a statistical prior of what sounds are more or less likely to follow other sounds).

To quantify the quality of reconstruction, we used the preferred method of Herff and colleagues: decomposing the true and synthesized audio into time-frequency bins, and then measuring the correlation between the true and synthesized audio. Specifically, 50 ms windows of the audio (advanced by 40 ms with each step, resulting in 10 ms window overlaps) were transformed into the spectral domain onto the Mel scale (Stevens *et al* 1937) using the Librosa package (Mcfee *et al* 2019). Forty overlapping triangular Mel filters spanning 0 to 16 kHz were used, and the resulting power in each time-frequency bin was converted to decibels. This yielded 40 vectors (one for each frequency bin) for each of the true and synthetic time-varying spectral power; we then calculated the Pearson correlation coefficient between each frequency's true and synthetic vectors. As in (Herff *et al* 2019), the final reconstruction quality metrics reported are the mean across these 40 individual frequency bin correlations.

To measure chance performance, this procedure was repeated 100 times but with the 'best match' speech units randomly selected from the training data, rather than selecting the unit with the most similar neural feature vector.

### 3. Results

#### 3.1. Single electrode modulation when producing speech

We first assessed single electrode phoneme tuning properties by measuring firing rate changes between the instructed delay period (when participants first read a short word) and around speech onset (when they spoke it out loud in response to a go cue). For each electrode, we examined a 500 millisecond window of delay period activity just prior to the go cue and a 100 millisecond window centered on each phoneme's voice onset time. We then calculated average firing rates within each window (figure 2(A)) and tested the significance of FR changes across these two time windows (permutation sign-test, 1000 permutations; uncorrected) for all phoneme classes (figures 2(B), (D)). To maintain statistical independence of samples, if the same phoneme class occurred multiple times within a trial, we randomly selected only one occurrence. Nearly all electrodes showed firing rate modulations to speaking at least one phoneme (156/158 electrodes for T5, 179/179 for T11). A sizable minority of electrodes showed tuning to at least half of all phoneme classes (40/158 electrodes for T5, 41/179 for T11, figures 2(E)–(F). Across electrodes and phonemes, significant firing rate changes largely reflected increasing firing rates around voice onset (78% and 86% of significant changes for T5 and T11

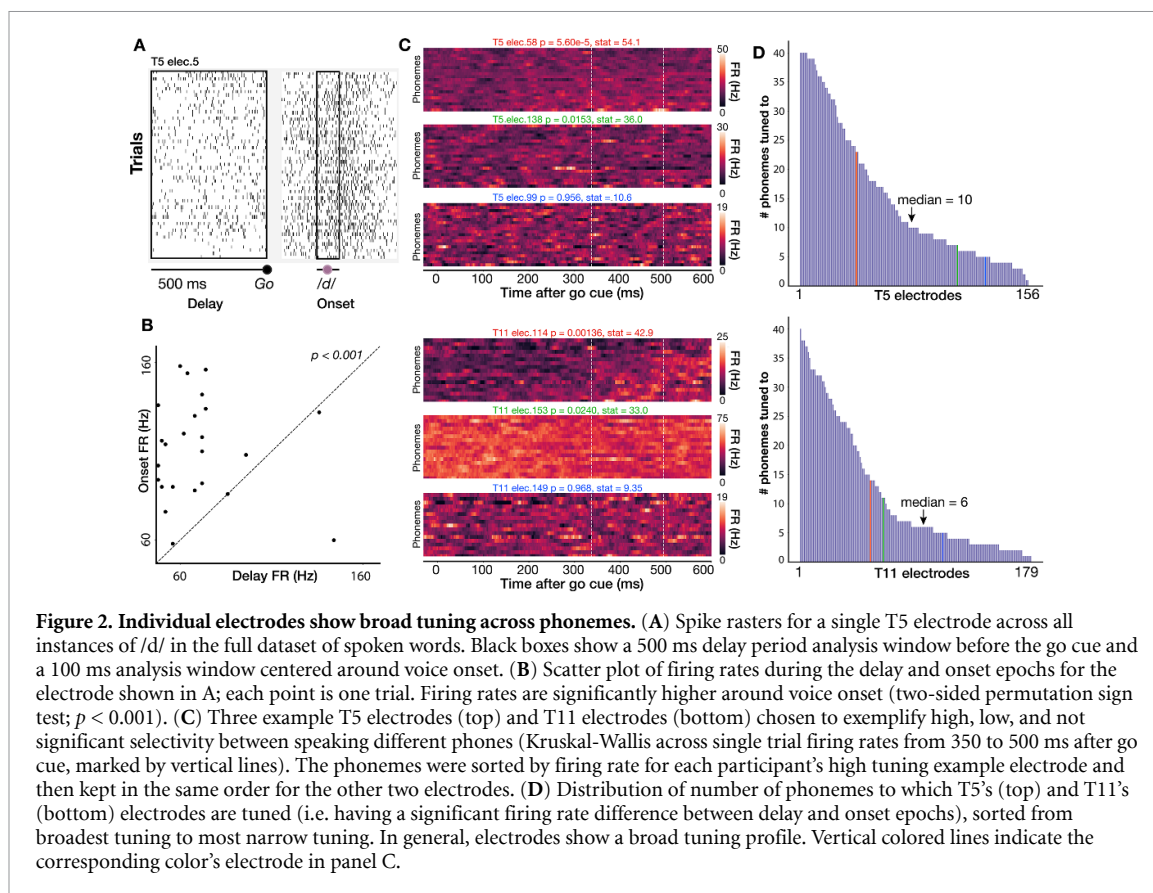


**Figure 2. Individual electrodes show broad tuning across phonemes.** (A) Spike rasters for a single T5 electrode across all instances of /d/ in the full dataset of spoken words. Black boxes show a 500 ms delay period analysis window before the go cue and a 100 ms analysis window centered around voice onset. (B) Scatter plot of firing rates during the delay and onset epochs for the electrode shown in A; each point is one trial. Firing rates are significantly higher around voice onset (two-sided permutation sign test;  $p < 0.001$ ). (C) Three example T5 electrodes (top) and T11 electrodes (bottom) chosen to exemplify high, low, and not significant selectivity between speaking different phones (Kruskal-Wallis across single trial firing rates from 350 to 500 ms after go cue, marked by vertical lines). The phonemes were sorted by firing rate for each participant's high tuning example electrode and then kept in the same order for the other two electrodes. (D) Distribution of number of phonemes to which T5's (top) and T11's (bottom) electrodes are tuned (i.e. having a significant firing rate difference between delay and onset epochs), sorted from broadest tuning to most narrow tuning. In general, electrodes show a broad tuning profile. Vertical colored lines indicate the corresponding color's electrode in panel C.

respectively). Thus, a dominant feature of these data was broadly tuned firing rate increase after the go cue, consistent with our previous intracortical multielectrode recordings (Stavisky *et al* 2019) and prior ECoG recordings in ventral sensorimotor cortex (Bouchard *et al* 2013, Mugler *et al* 2018).

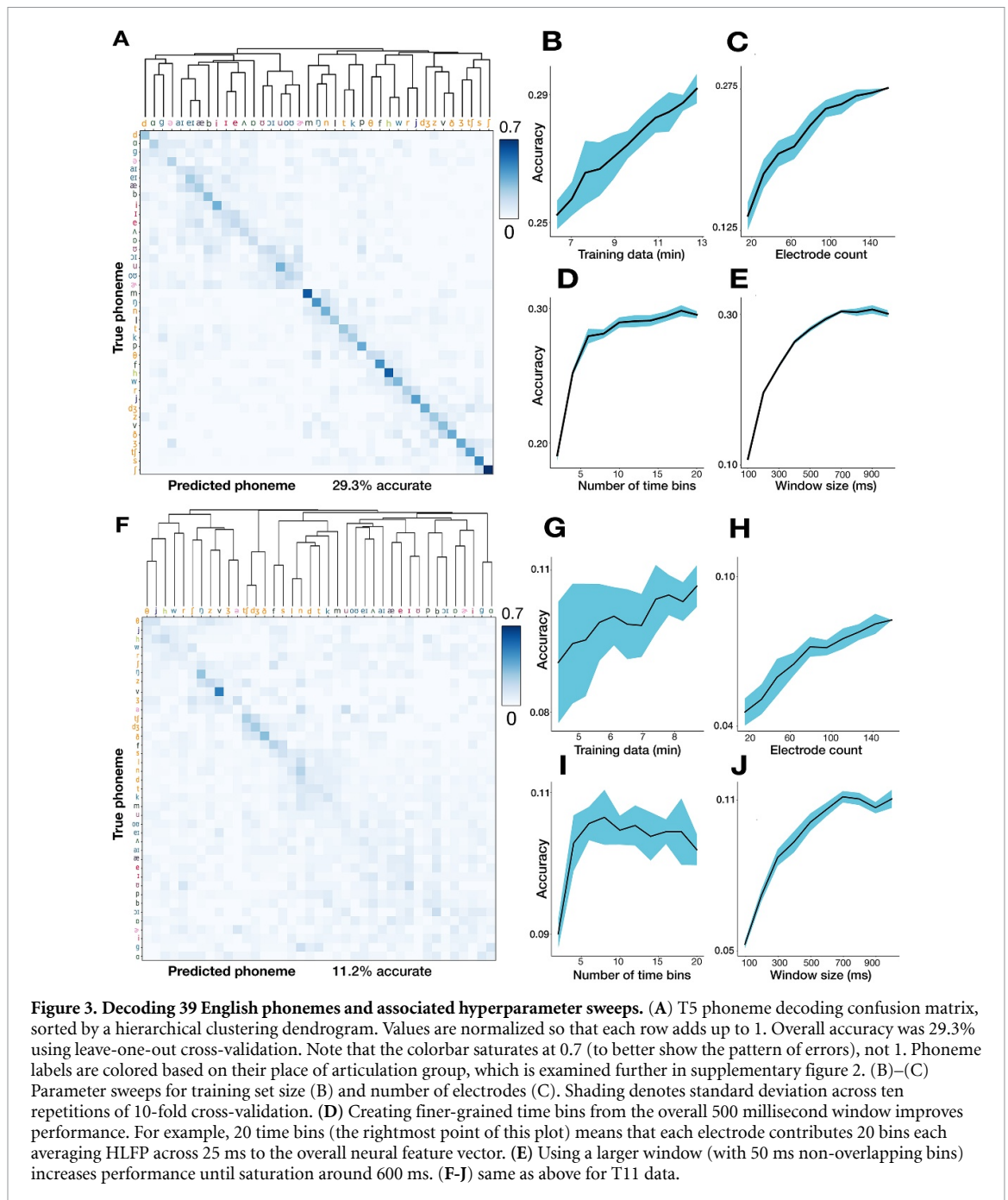
These data did not contain strong preparatory activity or phoneme discriminability during the instructed delay period. Therefore, in the rest of this study we focus on decoding the activity immediately preceding and during overt speaking. Speech epoch firing rates (averaged across electrodes and a 1 s window centered on each phoneme utterance's onset) were  $18.1 \pm 35.0$  Hz for T5 (mean  $\pm$  s.d.) and  $10.6 \pm 27.6$  Hz for T11.

### 3.2. Decoding English phonemes using neural population activity

We next sought to assess the utility of these signals for a speech BCI by decoding (offline) the identity of individual phoneme utterances from the neural activity across all functioning electrodes. We trained logistic regression classifiers with neural data and phoneme labels across all utterances ( $\sim 14$  total minutes data) and assessed cross-validated classification accuracy across 39 phonemes. Our first major observation was that although TC-spikes contained substantial information about phoneme identity (14.8% accuracy for T5, 7.9% accuracy for T11,  $p < 0.002$  compared to chance), classification was

much more accurate when decoding HLFP (125–5000 Hz): 29.29% and 11.22% for T5 and T11 respectively (figures 3(A), (F)). This is consistent with our previous study decoding a small number of syllables spoken by T5 (Stavisky *et al* 2018) and previous arm and hand decoding/BCI studies (Stark and Abeles 2007, Bouton *et al* 2016, Pandarinath *et al* 2017, Zhang *et al* 2018, Nason *et al* 2020) employing Utah arrays.

The superior performance of HLFP decoding may reflect this neural feature more robustly capturing spiking activity from more neurons in the local vicinity of each electrode (Asher *et al* 2007, Buzsáki *et al* 2012, Waldert *et al* 2013, Nason *et al* 2020). However, our result does not imply that there is universally more information in the spike band power than in the action potentials, and especially not in the case where isolatable single neuron activity would be observed on every electrode. Rather, the ensemble HLFP across electrodes may contain more decodable information than the ensemble spikes in a scenario where many electrodes do not record isolatable single units or even large amplitude multiunit TCs (which will often be the case for chronic electrode arrays, given today's technology). Furthermore, combining the activities of several neurons by decoding TC-spikes (an information-destroying aggregation that will also occur in the HLFP signal), has been shown in practice to not substantially reduce the accuracy of decoding movements from motor cortex



(Chestek *et al* 2011, Christie *et al* 2015, Trautmann *et al* 2019). Since HLFP decoding outperformed TC-spikes decoding in these data, for the remaining analyses we will focus on this more informative neural feature.

To better understand how phoneme decoding varied as a function of the quantity and temporal granularity of the input intracortical data, we measured performance as a function of increasing training dataset size, electrode count, and the number of time bins within an overall 500 millisecond window. Increasing accuracy as a function of both more training data (figures 3(B), (G)) and more electrodes used (figures 3(C), (H)) did not show performance saturation. Importantly, this indicates that

a path to improve intracortical speech BCI performance would be to collect more data and implant more electrodes. Taking advantage of time-varying structure by dividing each utterance's neural window into more time bins substantially increased performance (figures 3(D), (I)). This observation is in accordance with prior ECoG decoding work (Ramsey *et al* 2018). Unlike T5's almost monotonic improvement with more fine-grained time bins, T11's classification performance saturated at ten bins (each 100 ms long) and then declined. This trend likely follows from the lower signal-to-noise ratio (SNR) and lower overall firing rates in T11's recordings, in which case short time bins will exacerbate noise in the inputs and reduce decoding accuracy.

Using a total time window of approximately 600 milliseconds maximized performance; this agrees with a similar analysis by Mugler and colleagues (Mugler *et al* 2014). This optimal decoding window is substantially longer than the typical phoneme duration (supplementary figure 1) and likely reflects that the motor cortical correlates of producing each phoneme are longer than that phoneme's audible duration (Tourville and Guenther 2011; Hickok 2012). However, this increasing classification accuracy when using longer time windows should be interpreted with caution for at least two reasons. First, given the limited dictionary size in this study (420 words), increasing the decoding window may allow the classifier to exploit neural correlates of adjacent phonemes in a way that is not representative of what could be expected during open vocabulary decoding. Second, overly long time bins may introduce problematic delays if used in a closed-loop speech BCI (e.g. by delaying when decoded sounds/words are synthesized/typed) (Rabbani *et al* 2019). While the user might be able to compensate with slower speech, this would reduce the maximum potential communication rate; thus, the choice of online decoding window duration will likely reflect a speed versus accuracy trade-off.

Although phoneme prediction was above chance in both participants, classification accuracy was much higher in T5 than in T11. This result is consistent with ongoing efforts to characterize these T11 signals' relationship to a variety of actualized and attempted movements (including attempted arm and hand movements), where preliminary findings indicate that T11's arrays modulate substantially during movements, but exhibit less specificity than the T5 recording. This could reflect differences either in array placement or in modulation specific to this area of cortex in this participant. Given this lack of phoneme-related neural specificity in T11's recordings, we believe that T5's signals more closely approximate those that would be available in ventral areas of motor cortex that would be recorded from in future work specifically centered on building a speech prosthesis. Thus, here the subsequent analyses exploring phoneme decoding in more depth are restricted to the more informative T5 dataset.

To more directly compare the information content in T5's intracortical recordings to a prior ECoG study reporting what is (to our knowledge) the highest accuracy in decoding phonemes within stand-alone short words (Mugler *et al* 2014), we attempted a closely matched comparison to that study. This was facilitated by our having deliberately used a similar set of prompted words: 232 of our words were also used by Mugler and colleagues (Mugler *et al* 2014), and we picked replacements for the missing 80 words by choosing similar words from our (larger) word set (see 2.2: *Many words task*). For this analysis we also restricted our trials to match the trial count of the participant with the highest performance

in Mugler and colleagues (Mugler *et al* 2014) and used an equivalent 600 millisecond window centered on voice onset (supplementary figure 2). Decoding vowels and consonants separately as in (Mugler *et al* 2014), the T5 dataset accuracy was 36.8% across 24 consonant classes (vs. 36.1% in Mugler *et al*'s best participant) and 27.7% across 16 vowels classes (vs. 23.9%).

In the previous analyses we used logistic regression decoding in the interest of pragmatic considerations (compute time for parameter sweeps) and facilitating comparison to previous work (Mugler *et al* 2014). However, we recognize that additional performance may be gained by employing modern and powerful machine learning techniques, which may be particularly well-suited for decoding the dynamic neural activity underlying speech (Livezey *et al* 2019, Angrick *et al* 2019, Anumanchipalli *et al* 2019). To that end, we also decoded T5's phonemes dataset using an RNN with data augmentation (see 2.8 *RNN decoder*). However, this resulted in only a modest performance improvement (33.4% accuracy versus 29.6% for a logistic regression with matched input data; Supplementary figure 3).

### 3.3. A neural realignment strategy to correct for systematic voice onset biases between phonemes

We next turn to the first of two potential confounds by which studying audible speech may artifactually inflate the accuracy of decoding the corresponding neural data. Recall that, as per standard practice, we defined the start of each phoneme utterance based on the audio recording. This approach makes an important assumption: insofar as detectable speech sound lags the start of the underlying process of speech production, this lag is consistent across different phonemes. However, this assumption is unlikely to hold under most models of what motor cortex encodes. Specifically, if neural activity reflects articulatory movements (Lotte *et al* 2015, Chartier *et al* 2018, Mugler *et al* 2018, Stavisky *et al* 2019), then there may be across-phoneme differences between when articulatory movements start versus when the phoneme is clearly audible.

Figure 4(A) presents empirical evidence of this problem by showing different time alignments to generate an example electrode's firing rates as T5 spoke different phonemes. In the left-most panel, neural data are aligned to the task go cue; note that these analyses only include the first phoneme of each word to facilitate aligning to the go cue or to the neural correlate of speech initiation, as described below. This example electrode's firing rate increased shortly after the go cue and was largely similar across phonemes, consistent with the presence of a large CIS (Kaufman *et al* 2016), upon speech initiation (Stavisky *et al* 2019). In addition to this general activity increase, there was also phoneme-specific

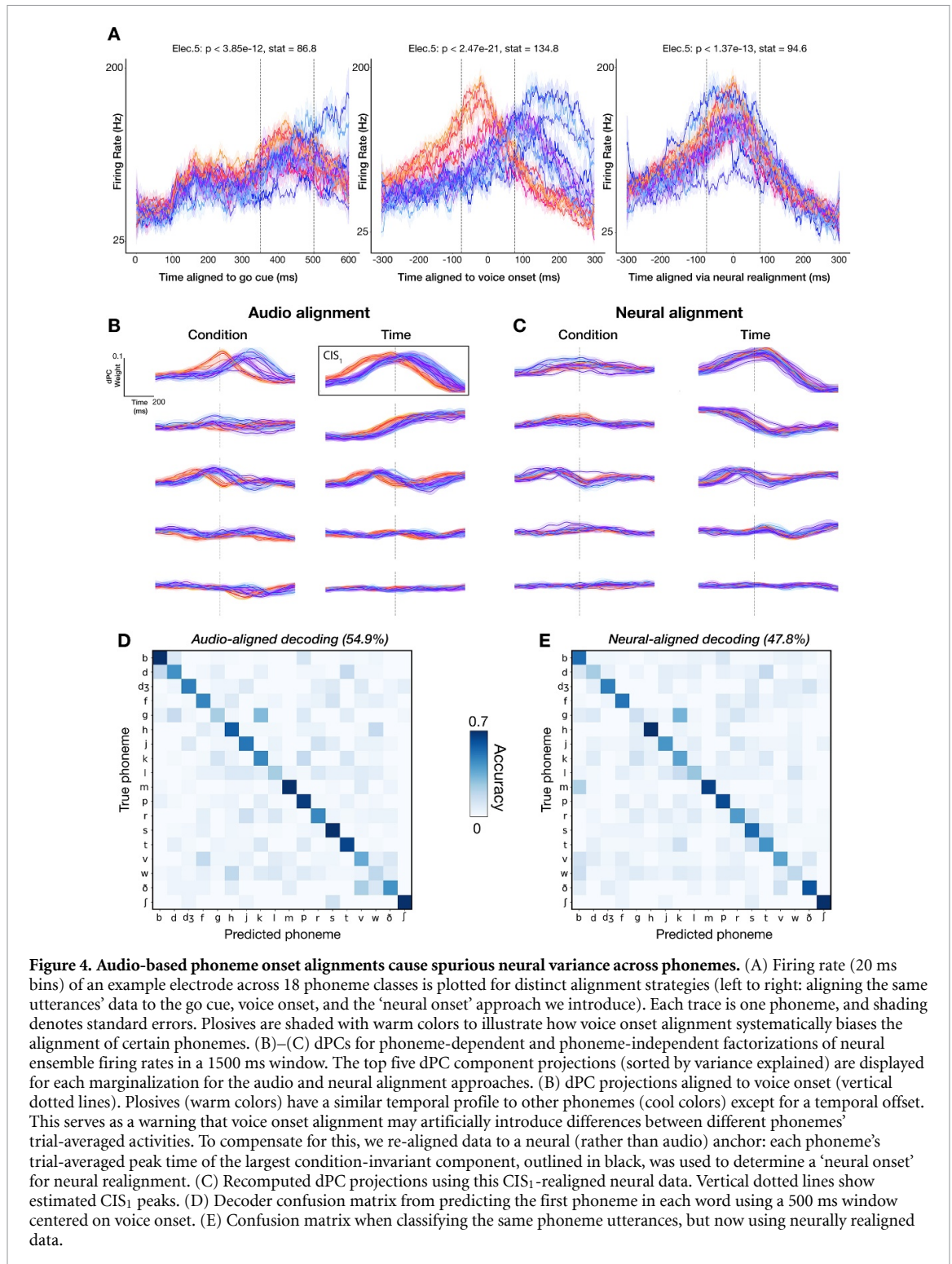


**Figure 4. Audio-based phoneme onset alignments cause spurious neural variance across phonemes.** (A) Firing rate (20 ms bins) of an example electrode across 18 phoneme classes is plotted for distinct alignment strategies (left to right: aligning the same utterances' data to the go cue, voice onset, and the 'neural onset' approach we introduce). Each trace is one phoneme, and shading denotes standard errors. Positives are shaded with warm colors to illustrate how voice onset alignment systematically biases the alignment of certain phonemes. (B)–(C) dPCs for phoneme-dependent and phoneme-independent factorizations of neural ensemble firing rates in a 1500 ms window. The top five dPC component projections (sorted by variance explained) are displayed for each marginalization for the audio and neural alignment approaches. (B) dPC projections aligned to voice onset (vertical dotted lines). Positives (warm colors) have a similar temporal profile to other phonemes (cool colors) except for a temporal offset. This serves as a warning that voice onset alignment may artificially introduce differences between different phonemes' trial-averaged activities. To compensate for this, we re-aligned data to a neural (rather than audio) anchor: each phoneme's trial-averaged peak time of the largest condition-invariant component, outlined in black, was used to determine a 'neural onset' for neural realignment. (C) Recomputed dPC projections using this CIS<sub>1</sub>-realigned neural data. Vertical dotted lines show estimated CIS<sub>1</sub> peaks. (D) Decoder confusion matrix from predicting the first phoneme in each word using a 500 ms window centered on voice onset. (E) Confusion matrix when classifying the same phoneme utterances, but now using neurally realigned data.

information as indicated by significant firing rate differences between phonemes in the epoch from 350 ms to 500 ms after the go cue. These data also suggest that there were not large systematic differences in the reaction time when speaking words that start with different phonemes. In stark contrast, the figure 4(A) center panel shows the same trials aligned to audio-derived voice onset time. The firing rate traces for plosives (/p/, /b/, /k/, /g/, /t/, and /d/) are shown with warm colors to better highlight a systematic onset

timing bias. These phonemes' firing rates follow a similar time-course to the other phonemes', except for a time offset, which leads to much greater differences across phonemes in an analysis epoch of the same duration (150 ms) now centered on voice onset. These plosive phonemes involve a temporary constriction of airflow (which produces little sound), followed by a rapid (and very audible) release of air, thereby increasing the latency between when phoneme production starts (e.g. movement of the lips) and when

the voice onset is detected. This example vividly illustrates that using audio data to mark the start of each phoneme utterance can introduce systematic timing biases that appear as spuriously accentuated differences across phonemes.

As an alternative to audio-derived voice onset, we attempted to detect phoneme onsets directly from the neural data. We used the largest variance phoneme-independent component of the neural population signal, the 'CIS<sub>1</sub>', as a speech activity onset indicator. This linear readout was previously found to be time-locked to attempted motor activity (Kaufman *et al* 2016), including during speaking (Stavisky *et al* 2019). Since the CIS<sub>1</sub>'s temporal profile should be largely invariant across speaking different phonemes, we can perform a 'neural realignment' by aligning CIS<sub>1</sub> peaks across conditions. To do so, we used the demixed PCA (Kobak *et al* 2016) dimensionality reduction technique to decompose and summarize the neural ensemble activity into a smaller number of condition-invariant and condition-specific components. Figure 4(B) shows ten of these population modes. The time-courses of these components across phonemes appear very similar except for temporal offsets, providing a population-level corroboration of the previous single electrode example. Once again, the early peaking traces correspond to plosives, suggesting that audio-based timing cues are systematically biased across different phoneme classes and that aligning to voice onset introduced spurious variance into our trial-averaged neural activity.

We then used each phoneme class' CIS<sub>1</sub> peak to identify a temporal shift relative to its audio voice onset. This allowed us to realign the corresponding neural data to this 'neural onset'. For instance, /b/ had a shift of -20 milliseconds; thus, for all trials with words that start with /b/, we shifted our neural data 20 milliseconds forward in time. Performing dPCA again on these realigned data (figure 4(C)), both the condition-invariant and the condition-specific components were more similar across phoneme classes. The right-most plot of figure 4(A) shows the same example electrode, now realigned using this CIS<sub>1</sub>-derived neural onset time. Here the time-courses of each phoneme appear more similar than when aligning to audio-derived voice onset, but there were still significant differences between phonemes.

### 3.4. Classification is weakly affected by audio alignment-based phoneme onset timing bias

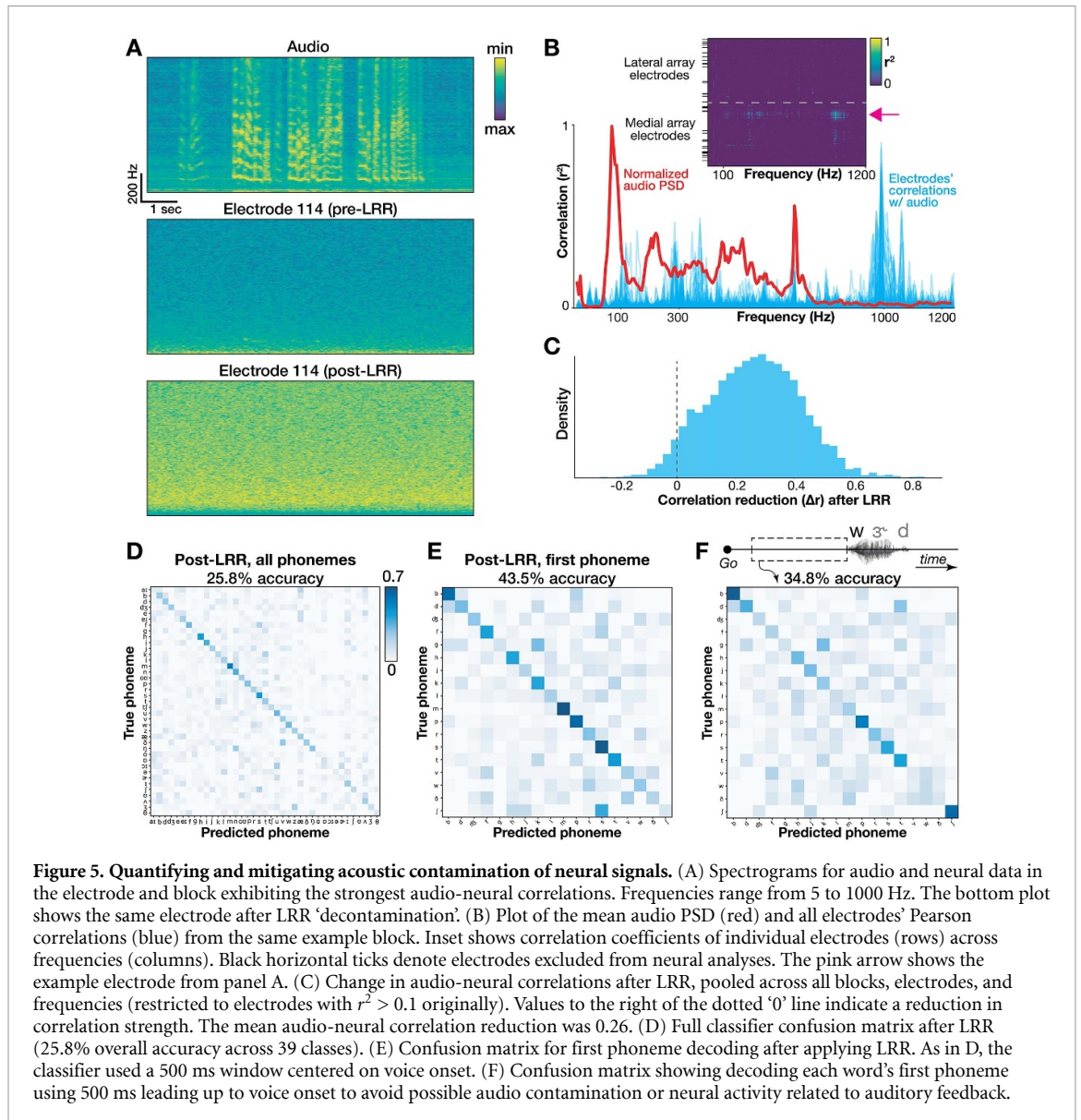
In the previous section we identified a phoneme timing bias from audio-derived onset labeling, and also demonstrated a method to correct for this bias (at least for the first phoneme of a word) using neurally-derived onset labeling. This allows us to now quantify how much phoneme onset biases can affect decoding audio-labeled phonemes by enabling a classifier to take advantage of spurious neural variance across phoneme classes.

To measure the impact of this confound, we trained separate decoders to classify the first phoneme of T5's spoken words using 1) the original neural data windows, which were aligned to voice onset as in figure 3, and 2) the realigned neural data windows obtained using CIS<sub>1</sub> peak alignment. For both procedures, we used the same preprocessing steps as before (see 3.2). Decoding each word's first phoneme from neural data time windows centered on neurally-derived phoneme onsets yielded 47.8% accuracy across 18 classes (figure 4(E)), as compared to 54.9% using windows centered on audio-derived phoneme onsets (figure 4(D)), a relative decrease of 12.9%. This indicates that audio-derived phoneme onset biases inflate overt speech decoding accuracies, but only modestly so.

### 3.5. Classification is weakly affected by microphonic artifact and is possible before voice onset

The second potential confound stemming from studying neural correlates of audible speech is that speaking could mechanically jostle components of the electrophysiology recording system, which would interact with ambient electromagnetic fields to generate small electrical currents that affect the final voltage measurement (i.e. microphonic pickup). This could be a larger or smaller effect, or no effect at all, depending on electromagnetic shielding (e.g. of cables), ambient electromagnetic power (e.g. other powered devices nearby, including lighting) and how recording components are stabilized (e.g. cables immobilized or not). There is also the possibility that there is an acoustic effect, but that it arises from some other mechanism that is not understood. To identify if audio contamination was potentially impacting classification performance, we implemented four different analyses.

We first looked for frequency-specific correlations between audio and neural signals, as in (Roussel *et al* 2020). We computed spectrograms for simultaneous speech audio (microphone) recordings and each electrode's activity (figure 5(A)). This yielded a set of time series containing frequency-specific signal power from 5 to 1200 Hz. We isolated time snippets with audible speech (see 2.10: *Quantifying acoustic artifact and Linear Regression Reference (LRR) decontamination*) and correlated these electrode and audio PSD time series at each frequency. If microphonic pickup had heavily contaminated our recordings, then the most prominent audio frequencies would most likely induce oscillations in the electrode signal at the corresponding frequency and manifest as stronger correlations with the associated 'neural' signal power at those frequencies. Plotting the mean PSD across speech timepoints alongside our electrodes' correlations for an example block, we found strong electrode-audio correlations across a



range of frequencies (figure 5(B)) with a max correlation  $r = 0.953$  across all  $192 \text{ electrodes} \times 240 \text{ frequencies} = 46\,080$  comparisons, and a median  $r = -0.002$ . This implies that our neural recordings contain microphonic contamination in at least some frequency bin(s) on some electrode(s). However, inspecting the example electrode which had the strongest overall audio-neural correlation (figure 5(A)), we still see little contamination visible to the eye. This contrasts with the striking obvious contamination in some of the recordings analyzed in (Roussel *et al* 2020). The figure 5(B) inset summarizes the correlation with audio across all electrodes, and reveals a small set of electrodes with higher audio-neural correlations, all on the same (medial) array.

Second, to more directly test whether mechanical vibrations in the speech range could, in principle, affect our recordings, we performed a positive control where we intentionally applied a mechano-acoustic stimulus to the recording setup. During a separate

research session with participant T5, we held an activated 340 Hz or 480 Hz tuning fork either in the air in front of the (fully connectorized) participant (supplementary figure 4(A)), or pressed the activated fork’s stem to his head near the connector pedestals (supplementary figure 4(B)), directly to the pre-amplifiers (supplementary figure 4(C)), or directly to the connector cables (supplementary figure 4(D)). We reasoned that since a tuning fork applies the majority of its mechanical energy into the recording apparatus at a specific frequency (unlike speech), and is unlikely to evoke biological neural oscillations in a motor cortical area at that same specific frequency, then a sharp increase in recorded signal power at the fork’s vibration frequency would clearly indicate the presence of an artifact. We did indeed observe such an artifact on some medial array electrodes when the tuning fork was applied to the pre-amplifier and cable, the two conditions in which there was putatively the most mechanical energy being transferred

into the recording apparatus. This result demonstrates that our measurement and analysis methods do have the sensitivity to detect acoustic contamination, at least at these frequencies and amplitudes. We do not purport to equate this artificial tuning fork stimulation to the acousto-mechanical interaction between the participant speaking and the recording system; rather, this result, which is consistent with (Roussel *et al* 2020), merely shows that there exist conditions under which artifactual acoustic contamination is possible. This lends support to the aforementioned suspicion that some of the speech-correlated neural activity was due to acoustic contamination.

Third, as a conservative decoding analysis that would avoid acoustic contamination, we extracted a 500 millisecond neural window just prior to each word, before speech onset. Since this neural activity precedes audible audio signals, it cannot be polluted by microphonic pickup. This analysis also serves as a control that excludes the potential contribution to decoding by neural processing of auditory feedback in this motor cortical area. Decoding these pre-voice neural windows for each word's first phoneme yielded a cross-validated (20 fold) classification performance of 34.8% across 18 classes (figure 5(F)), well above chance performance ( $p < 0.002$ ; permutation test, 500 permutations). For comparison, using a 500 ms neural window centered on the phoneme's voice onset (which we expect to better capture phoneme production-specific neural activity, in addition to potential acoustic contamination and auditory feedback) yielded an accuracy of 54.9% (figure 4(D)).

Fourth, we implemented a denoising procedure, Linear Regression Reference (LRR) (Young *et al* 2018), which aims to mitigate acoustic contamination of the neural signals. LRR works by subtracting out predictable signals shared across many electrodes (which is what we would expect from microphonic pickup) from each electrode's activity. A linear regression model estimates each electrode's activity using instantaneous activity from all other electrodes; this prediction is then subtracted from that electrode's original time series to yield the denoised estimate. This approach was first applied in (Young *et al* 2018) to remove electrical artifacts induced during intracortical microstimulation. Here we applied the method to putative acoustic contamination by fitting regression models to bandpass-filtered (125–5000 Hz to match our HLF neural feature) voltage signals. Figure 5(A) shows an example electrode's activity before and after LRR, while supplementary figure 4(E) demonstrates that this technique successfully removes much (but not all) of the artifact introduced in the tuning fork positive control. Following LRR, we observed a substantial reduction in audio-neural correlations (figure 5(C)), indicating that the procedure was mitigating acoustic

contamination. At the same time, there was only a small reduction in cross-validated accuracy decoding all phonemes (reduction from 29.3% to 25.8%, figure 5(D)), indicating that the procedure was not eliminating much phoneme-specific information. However, we note that the LRR technique does not guarantee that all acoustic contamination is eliminated (which would cause us to under-estimate the contribution of microphonic pickup to decoding accuracy), and it also can subtract out genuine neural signal that is shared across electrodes (which would cause us to over-estimate the contribution). Thus, these results should be viewed as just one piece of evidence towards estimating the effects of acoustic contamination in overt speech decoding studies.

In summary, our results support the concern raised by (Roussel *et al* 2020) that microphonic artifacts are present in intracortical and ECoG recordings during overt speech. These audio-driven signals may well have somewhat increased the phoneme classification accuracies in this study. However, our further analyses described in this section bracket this potential artifactual contribution as small and, critically, show that we can decode phonemes even before audible voicing (figure 5(F)). This agrees with our prior findings that neural activity in this area modulates in response to unvoiced orofacial movements (Stavisky *et al* 2019).

### 3.6. Classifier confusions correlate with place of articulation groupings

We now return to the observation that when sorting our decoder confusion matrices based on the results of agglomerative hierarchical clustering (Sokal & Michener 1958), the resulting dendrograms suggest divisions across phonemes relating to their phonemic groupings (figure 3(A); e.g. broad vowel-consonant divisions). A permutation test (see 2.7: *Logistic regression for phoneme classification*) revealed significantly higher confusion within place of articulation groups than between groups (supplementary figures 5(A)–(B);  $p < 0.005$ ), indicating that there was latent structure in our classifier errors putatively related to how similar the motoric demands of producing different phonemes were (Lotte *et al* 2015, Mugler *et al* 2018, Chartier *et al* 2018, Stavisky *et al* 2019). However, we identified in sections 3.3 and 3.4 that these classifier errors were somewhat affected by systematic across-phoneme differences in labeled voice onsets. This raises the concern that the pattern of decoding errors could be related to similarities in phonemes' latencies between speech production initiation and voice onset, rather than place of articulation *per se*. We therefore repeated the place of articulation grouping analysis, but now applied to classifier errors from predicting the first phoneme of each word using neural alignment (as described for figure 4). We again observed higher confusion within place

of articulation groups (supplementary figures 5(C)–(D);  $p < 0.005$ ), suggesting that this error structure was not just an artifact of voice onset bias.

### 3.7. Speech synthesis using the ‘Brain-to-Speech’ unit selection method

In this work we have primarily evaluated the feasibility of using intracortical signals to decode discrete phonemes, which could be strung together by a speech BCI to generate audio or text. However, another approach for implementing a speech BCI is to directly synthesize speech sounds (Anumanchipalli *et al* 2019, Angrick *et al* 2019, Herff *et al* 2019). To more comprehensively test the suitability of intracortical array signals for a proof-of-concept speech BCI, we also applied a recently-published speech synthesis technique, termed ‘Brain-to-Speech’ by Herff and colleagues (Herff *et al* 2019), to our data. This pattern matching approach compares each sliding window of neural data to a library of training data consisting of neural and corresponding audio data. At each time step, Brain-to-Speech selects the snippet of audio data corresponding to the best matching neural window; these snippets are then smoothly concatenated to generate a synthesized audio output. This method has a number of attractive attributes, including being fast and data-efficient to train; potentially reproducing the user’s own voice, including intonation and prosody, if ground truth speech training data is available; and being very fast to compute (i.e. amenable to real-time use). Typically, such unit selection techniques (Hunt and Black 1996) select the next unit (here, an audio snippet) based both on a ‘target cost’, i.e. how well the input data (neural features) match each unit in the training library, and a ‘concatenation cost’ that uses a statistical model to evaluate how likely each unit would be given the previously selected units. However, as in (Herff *et al* 2019), here we did not use a concatenation cost in order to more directly test the information content of the neural data alone, without the additional benefits of statistical priors which would vary depending on the specific speech BCI application.

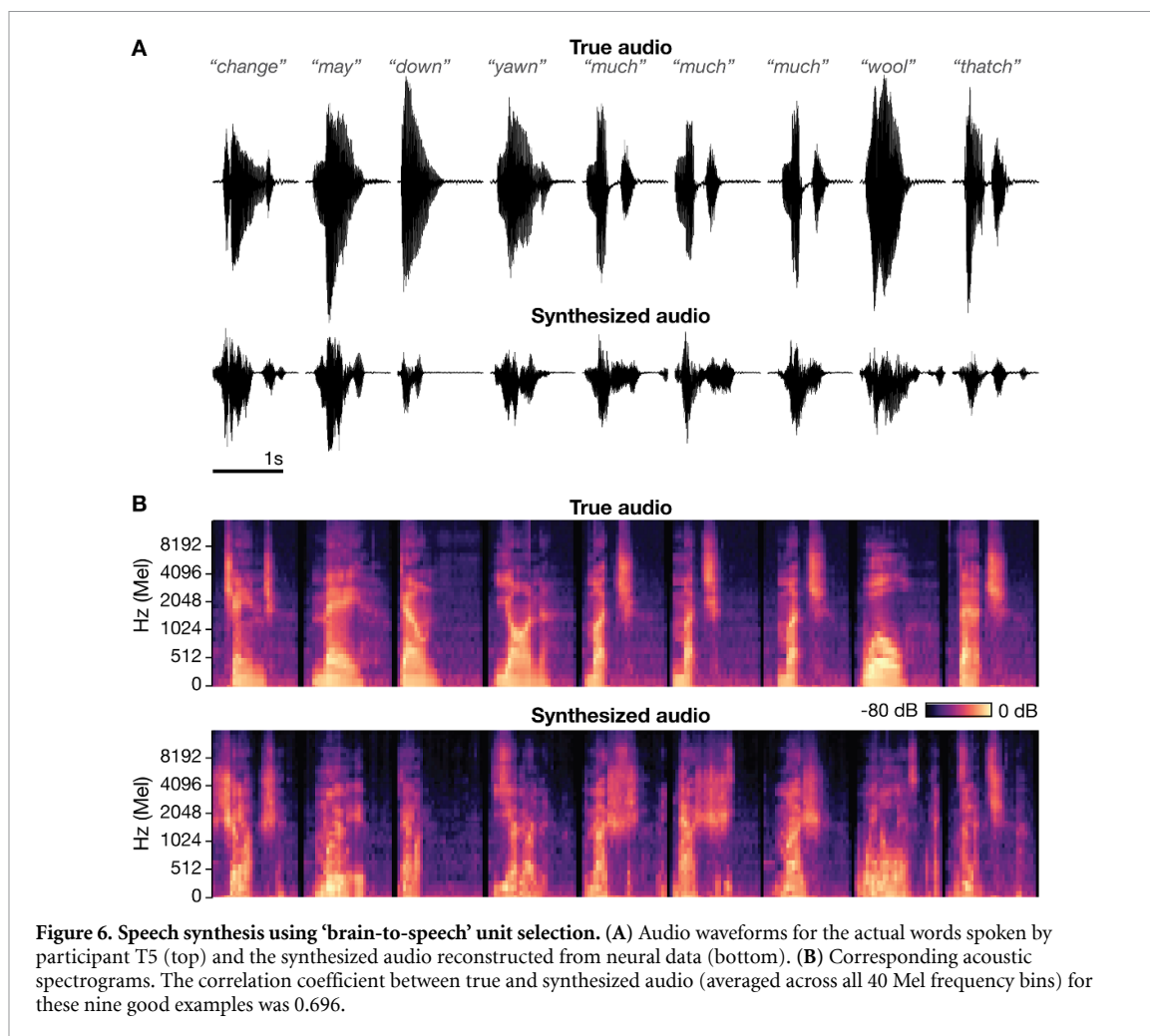
Figure 6 shows the result of applying this speech synthesis technique (offline) to the T5 dataset. As in (Herff *et al* 2019), good examples were chosen to showcase that in some cases the reconstructed audio is borderline intelligible. We quantified the reconstruction accuracy by decomposing the synthesized speech into time and frequency bins (40 logarithmically-spaced Mel-scale bins that approximate the human perception of speech) and calculating the correlation coefficient between the true and synthesized audio’s time-varying representation within each frequency bin. Averaging across all the data and all 40 bins, the mean correlation was 0.523. Chance performance ranged from 0.019 to 0.038, with a mean of 0.027. For comparison, using the same performance metric, Herff and colleagues report an accuracy of  $r = 0.574$

for the best participant in their ECoG study, and  $r = 0.246$  averaged across all six participants. This indicates that intracortical signals are also competitive with ECoG for this speech synthesis approach. Supplementary Audio 1 contains the true and synthesized audio for 47 *good* example words (the first nine of which are shown in figure 6). Supplementary Audio 2 presents another 47 *randomly* chosen example words which demonstrate that most synthesis trials were not intelligible.

## 4. Discussion

The present results indicate that decoding speech from intracortical arrays is a promising future direction for developing BCIs to restore lost speech. The phoneme classification accuracy and speech synthesis results demonstrated in the participant with more informative signals (T5) is similar to work performed with ECoG arrays that spanned a wide swath of speech-related cortical areas (Mugler *et al* 2014, Livezey *et al* 2019, Herff *et al* 2019). This is despite the limited spatial coverage of the present study’s Utah arrays (10 x 10 grid of electrodes spanning 4.0 mm x 4.0 mm; array backplane is 4.2 mm x 4.2 mm) and their sub-optimal placement outside traditional speech areas. This accuracy also exceeds a prior intracortical phoneme decoding study which used fewer electrodes and reported 21% accuracy across 38 phonemes (Brumberg *et al* 2011). However, we note the lower accuracy in the second participant (T11), and the overall gap between either participant’s decoder performance and the close to 100% accuracy one would aspire to for a speech BCI that approaches a healthy speaker’s capabilities. Thus, while we find these results encouraging, we do not believe that these dorsal precentral gyrus signals from two Utah arrays are sufficient to support fluent open-vocabulary communication using a speech BCI; rather, we view these results as a proof-of-concept demonstration that the intracortical approach is competitive with ECoG, and as motivation for future work using more electrodes placed in ventral speech areas.

As in prior ECoG studies (Mugler *et al* 2014, Moses *et al* 2019), we found that classifier errors exhibited articulatory structure (supplementary figure 5). Phonemes spoken with similar place of articulation were more likely to be confused with one another compared to phonemes with different places of articulation. This suggests that the underlying neural signals relate to the movement of articulator muscles, broadly in line with ECoG studies (Mugler *et al* 2014, 2018, Lotte *et al* 2015, Chartier *et al* 2018, Moses *et al* 2019) and earlier work looking at spiking activity in this dorsal ‘hand knob’ area (Stavisky *et al* 2019). Assuming that our signals reflect articulator movements underlying speech, then the observed classification accuracy improvement from using multiple time bins likely reflects the increased



ability to discriminate the time-varying movements underlying speech production (Mugler *et al* 2014, Ramsey *et al* 2018, Chartier *et al* 2018). Future decoding approaches that seek to specifically assess and optimize performance with an eye toward eventual speech BCI applications may benefit from classifier cost functions and performance metrics tailored to speech perception, rather than treating all phoneme mistakes the same. For example, if the final BCI output is sound synthesis, then metrics based upon distortions of auditory spectral features (Anumanchipalli *et al* 2019) may be more informative: misclassifying similar sounding phonemes (e.g. /p/ and /b/) would be less damaging to overall speech comprehension compared to mistakes across groupings (e.g. /p/ and /r/).

We observed better performance classifying consonants versus vowels (supplementary figure 2), which was also seen in earlier ECoG studies (Brumberg *et al* 2011, Mugler *et al* 2014, Ramsey *et al* 2018, Livezey *et al* 2019), although the factors explaining this phenomenon may differ for different recording modalities. In our case, lower vowel decoding accuracy might arise from the dataset statistics: most of the words our participants spoke were three phonemes long with consonant-vowel-consonant

structure, resulting in more consonant training data. A second possibility is that the 500 millisecond decoding window used is short compared to the audio durations of vowels (supplementary figure 1(C), 319 ms on average for T5); the resulting neural features may therefore cover more of the relevant information for short duration consonants (173 ms on average for T5). Future work might consider a hierarchical classifier that first tries to decode vowel versus consonant, and then uses different window sizes accordingly. A third possibility is that the underlying articulator movements involved in vowel production are less well sampled by these recordings (Brumberg *et al* 2011). Definitely testing the latter hypothesis will require future recordings of simultaneous neural and speech articulator activity.

The improved decoding performance when using high-frequency LFP power (as opposed to TCs) suggests that local voltage fluctuations can support phoneme classification without a need for spike detection. Indeed, prior decoding work across a more limited set of syllables found no accuracy difference between HLFP or spike features (Stavisky *et al* 2018). The superior performance of HLFP in the present study's more demanding phoneme classification task is consistent with studies showing

that such spiking band power signals can capture more task-related information from local neuronal activity than threshold crossings, including on electrodes that do not record sufficiently high SNR action potentials for spike detection (Stark and Abeles 2007, Nason *et al* 2020). While this suggests that broadband LFP features are sufficient for high-performance decoding, we caution that microelectrode field potentials, which are largely dominated by local action potentials (Nason *et al* 2020), reflect different underlying physiological sources than ECoG surface electrode recordings. In addition to being located on the surface of the brain (instead of  $\sim 1.5$  mm below the surface), ECoG electrodes are much larger ( $\sim 1$  mm<sup>2</sup> disks, versus  $\sim 0.001$  mm<sup>2</sup> Utah array electrode tips) and ECoG studies analyze the high gamma LFP power in a range of  $\sim 65$  to 250 Hz (Bouchard *et al* 2013, Martin *et al* 2014, Mugler *et al* 2014, Cheung *et al* 2016, Chartier *et al* 2018, Dichter *et al* 2018, Ramsey *et al* 2018) (versus this study's 125 to 5000 Hz). Importantly, performance here was dependent on sampling a sufficiently high number of electrodes from the two arrays (figure 2(C)). Corroborating this finding, individual electrodes had broad tuning profiles across phonemes, with 25% (T5) and 23% (T11) of all electrodes showing significant tuning to at least half of the 39 phonemes.

Leveraging a more computationally expressive machine learning approach for phoneme classification, we obtained a modest performance improvement using an RNN (33.9% accuracy, compared to 29.6% using logistic regression). Figures 3(B), (G) indicate that performance had not saturated when increasing the number of electrodes or training data, and even more data should further improve classification accuracy, especially for deep learning methods (Livezey *et al* 2019). Nonetheless, these results indicate that in the present data-impooverished context, deep learning provides only a small improvement compared to a simpler linear decoder. This echoes a pair of recent studies which synthesized speech from a shared dataset using either neural feature angle comparison (low complexity; (Herff *et al* 2019)) or convolutional neural networks (high complexity and only a small improvement; (Angrick *et al* 2019)). Furthermore, it seems unlikely that arrays in the hand knob area would support a very high performance speech BCI, even with more electrodes or training data. Future efforts will benefit from access to ventral speech cortex as well as higher electrode counts that record from a larger neural population.

In this study we also characterized and addressed two confounds that may be endemic to decoding overt speech. The first has not, to the best of our knowledge, been specifically examined before: labeling speech start times based on voice onset can artificially boost decoding performance by introducing systematic timing differences across phoneme classes between the onset labels and the

true time when neural activity rapidly changes during speech production. This timing bias can be seen at the level of individual electrodes (figure 4(A)) and at the neural population level (figure 4(B)), and is consistent with the neural activity largely reflecting underlying articulatory movements (Bouchard *et al* 2013, Lotte *et al* 2015, Chartier *et al* 2018, Mugler *et al* 2018), rather than when these movements cause detectable sounds. A systematic discrepancy between voice and neural onset times was noted in a previous study (Jiang *et al* 2016), which also proposed decoders that exploit relative neural onset differences between phoneme-specific and phoneme-independent neural components. It has also been previously noted (Mugler *et al* 2014) that phoneme decoding accuracy is sensitive to the precision of onset timing labeling. Here, we realigned phonemes' analysis windows to an onset time derived from the neural population signals themselves to account for this experimental confound and demonstrated that high performance classification was still possible (47.8% accuracy across 18 classes, figure 4(E)). We anticipate that this neural realignment strategy will also work in other recordings that contain strong condition-invariant responses time-locked to the speaking task. Because we observed an appreciable difference between decoder performance with and without this neural realignment (a 12.9% reduction in accuracy when classifying the first phoneme of each word), we caution that future speech BCI work based on voice onset labels should take across-labels timing biases into account.

We additionally found evidence of a second confound: acoustic contamination in our electrode signals (Roussel *et al* 2020). Strong correlations between audio and 'neural' activity occurred at specific frequencies, particularly in a cluster of electrodes on our medial array. However, unlike the characteristic correlation peaks around the fundamental frequency (and harmonics) of the more contaminated datasets in (Roussel *et al* 2020), our correlations exhibited a less consistent relationship with T5's audio PSD. This discrepancy may arise from the relatively short snippets of speech we had access to (as opposed to continuous speech), or they may reflect differences in the mechanics of acoustic contamination between specific setups. Further supporting our findings, we observed strong vibrations in the relevant frequency bands of some electrodes when applying a tuning fork to both our participant's pre-amplifier and connector cable, consistent with the bench-top tests in (Roussel *et al* 2020). To account for this contamination, we implemented two different approaches: 1) classification of each word's first phoneme using pre-voice onset activity, and 2) the novel use of a decontamination procedure previously deployed for electrical stimulation artifact reduction (Young *et al* 2018). By decoding phonemes using only pre-voicing neural activity (figure 5(D)), 34.8% accuracy across 18

classes), we showed that our performance is not solely a product of acoustic contamination. By mitigating correlations through a re-referencing approach, we found that we could still decode phonemes with relatively high accuracy (25.8% across 39 classes, although see 4.1). Thus, our conclusions are similar to that of (Roussel *et al* 2020): microphonic pickup is a (manageable) nuisance for overt speech decoding studies, and that in a robust recording setup the majority of the measured voltage signals are biological and not artifactual.

#### 4.1. Limitations

In this study we classified neural activity snippets aligned to phoneme onset, as determined from the audio recording of spoken speech. A clinical speech BCI will need to identify speech elements (such as phonemes) from unlabeled, continuous speaking data. Our speech synthesis results are one step in this direction, but free-running phoneme decoding from intracortical neural activity is a key next step for future work. Recent work decoding continuous speech from ECoG recordings indicates that this is feasible (Herff *et al* 2015, Anumanchipalli *et al* 2019), and we anticipate that similar methods can be applied to intracortical recordings. While this presents a greater challenge, natural language processing methods may provide substantial help in the continuous regime (Li and Negoita 2018). In particular, leveraging the statistical structure of language may enable ‘denoising’ of a neural decoder’s initial outputs (Moses *et al* 2019, Willett *et al* 2020b). No such corrections were employed in this study, where we instead sought to understand ‘raw neural performance’ before applying any language model (the effectiveness of which will depend on the specifics of the speech BCI application, e.g. open vocabulary versus a more constrained vocabulary).

Our neural realignment procedure allowed us to disentangle the contribution of true (neural) variance across phonemes from that of spurious variance driven by systematic onset timing biases. While the results indicate relatively unimpaired performance following realignment (47.8% post-alignment vs. 54.9%, 18 distinct classes), this check was restricted to classifying the first phoneme due to unreliable neural timing signals for subsequent phonemes. It thus remains an open challenge to quantify and mitigate the effect of voice onset biases for the later phonemes of a word.

Our recordings show evidence of acoustic contamination, which most likely improves classification performance. While our LRR procedure was able to mitigate this contamination, some acoustic contamination was probably still present. Future directions could examine a related artifact mitigation method (O’Shea and Shenoy 2018), with which we anticipate similar results. The present correlation analysis also assumes that the process of sound wave conversion

into voltage signal fluctuations preserves frequencies, as opposed to shifting them around. While our tuning fork experiment suggests that this is approximately true (supplementary figure 5—although this is not necessarily the same mechanism underlying speech-induced acoustic contamination), we note that Roussel and colleagues observed a slight shift in correlation peaks for a participant with intracortical arrays relative to their voicing fundamental frequency.

Additionally, it is possible that neural signals relating to auditory feedback, as opposed to speech articulation, may drive some of the classification performance in this study. However, we were able to decode words’ first phonemes without an audible voicing activity and, in prior work (Stavisky *et al* 2019), we also found strong tuning to unvoiced orofacial movements. Together, these findings suggest minimal feedback-driven signals compared to articulatory information. Future studies are needed to definitively disentangle these two processes during attempted speech decoding.

These confounds complicate direct comparisons to previous work, as their extents may vary between different studies’ recording setups. Given the different corrections that can be applied (auditory feedback restriction, microphonic pickup controls, neural realignment, etc.) and combinations thereof, we therefore caution that the phoneme decoding and speech synthesis comparisons made here should not be viewed as exact, matched performance tests but rather ballpark estimates. With these points in mind, the demonstrated performance is at least comparable to prior studies (Brumberg *et al* 2011, Mugler *et al* 2014, Livezey *et al* 2019) and motivates further intracortical speech decoding work.

## 5. Conclusions

Taken together, our results indicate that the limited spatial coverage of current intracortical electrode arrays is more than offset by the high speech-related information provided by intracortical recordings. Our offline decode results suggest a lower bound on intracortically-driven speech BCI performance, since these arrays in a ‘hand/arm’ area of precentral gyrus were likely suboptimally placed for speech decoding, and the participants did not receive online feedback that they could use to beneficially adjust their neural activity. This study de-risks and motivates future work in which arrays are implanted into ventral speech cortex in participants who cannot speak.

## Acknowledgments

We thank participants T5, T11 and their caregivers for their generously volunteered time and effort as part of our BrainGate2 pilot clinical trial. We also thank Professor Marc Slutzky for providing the many words

list; our Stanford NPTL and NPSL group for helpful discussions; Beverly Davis, Erika Siauciunas, and Nancy Lam for administrative support; and Dr. Darrel Deo (Stanford, NPTL group) for providing RNN decoder code documentation.

Some of the computing for this project was performed on the Stanford High Performance Computing Cluster (Sherlock cluster). We thank Stanford University and the Stanford Research Computing Center for providing expert IT support for this computational resource where our primary compute node is housed.

This work was supported by an National Science Foundation Graduate Research Fellowship DGE-1656518 and Regina Casper Stanford Graduate Fellowship (G.H.W.); the A. P. Giannini Foundation, Wu Tsai Neurosciences Institute Interdisciplinary Scholars Fellowship, and Burroughs Wellcome Fund Career Award at the Scientific Interface (S.D.S.); Howard Hughes Medical Institute (F.R.W., D.T.A., and K.V.S.); Office of Research and Development, Rehab. R&D Service, Department of Veterans Affairs (B6453R, N2864C); NIDCD R01DC014034, NINDS UH2NS095548, NINDS U01NS098968, the Executive Committee on Research (ECOR) of Massachusetts General Hospital, MGH Deane Institute for Integrated Research on Atrial Fibrillation and Stroke (L.R.H.); NIDCD R01DC014034, NIDCD U01DC017844, NINDS UH2-NS095548, NINDS UO1NS098968, Larry and Pamela Garlick, Samuel and Betsy Reeves, Wu Tsai Neurosciences Institute at Stanford (J.M.H. and K.V.S.); NIBIB R01-EB028171 (S.D.); and Simons Foundation Collaboration on the Global Brain 543045 (K.V.S.).

### Declaration of interests

The MGH Translational Research Center has a clinical research support agreement with Neuralink, Paradromics, and Synchron, for which L.R.H. provides consultative input. JMH is a consultant for Neuralink Corp and Proteus Biomedical, and serves on the Medical Advisory Board of Enspire DBS. KVS consults for Neuralink Corp. and CTRL-Labs Inc. (part of Facebook Reality Labs) and is on the scientific advisory boards of MIND-X Inc. Inscopix Inc. and Heal Inc. S.D. consults for CTRL-Labs Inc. (part of Facebook Reality Labs). All other authors have no competing interests.

### ORCID iDs

Guy H Wilson  <https://orcid.org/0000-0003-0961-1994>

Sergey D Stavisky  <https://orcid.org/0000-0002-5238-0573>

Francis R Willett  <https://orcid.org/0000-0002-2652-8511>

Donald T Avansino  <https://orcid.org/0000-0002-7974-0153>

Jessica N Kelemen  <https://orcid.org/0000-0002-2779-0431>

Leigh R Hochberg  <https://orcid.org/0000-0003-0261-2273>

Jaimie M Henderson  <https://orcid.org/0000-0002-3276-2267>

Shaul Druckmann  <https://orcid.org/0000-0003-0068-3377>

Krishna V Shenoy  <https://orcid.org/0000-0003-1534-9240>

### References

- Abadi M et al 2016 Tensorflow: a system for large-scale machine learning *12th USENIX Symp. on Operating Systems Design and Implementation (OSDI 16)* 265–83
- Abbott L F and Dayan P 1999 The effect of correlated variability on the accuracy of a population code *Neural Comput.* **11** 91–101
- Ajiboye A B et al 2017 Restoration of reaching and grasping movements through brain-controlled muscle stimulation in a person with tetraplegia: a proof-of-concept demonstration *Lancet* **389** 1821–30
- Akbari H, Khalighinejad B, Herrero J L, Mehta A D and Mesgarani N 2019 Towards reconstructing intelligible speech from the human auditory cortex *Sci. Rep.* **9** 1–12
- Angrick M, Herff C, Mugler E, Tate M C, Slutzky M W, Krusienski D J and Schultz T 2019 Speech synthesis from ECoG using densely connected 3D convolutional neural networks *J. Neural. Eng.* **16** 036019
- Anumanchipalli G K, Chartier J and Chang E F 2019 Speech synthesis from neural decoding of spoken sentences *Nature* **568** 493–8
- Asher I, Stark E, Abeles M and Prut Y 2007 Comparison of direction and object selectivity of local field potentials and single units in macaque posterior parietal cortex during prehension *J. Neurophysiol.* **97** 3684–95
- Boersma P 2001 Praat, a system for doing phonetics by computer *Glott. Int.* **5** 341–5
- Bouchard K E and Chang E F 2014 Neural decoding of spoken vowels from human sensory-motor cortex with high-density electrocorticography *Conf. Proc. Ann. Int. Conf. of the IEEE Eng. Med. Biol. Soc.* pp 6782–5
- Bouchard K E, Mesgarani N, Johnson K and Chang E F 2013 Functional organization of human sensorimotor cortex for speech articulation *Nature* **495** 327–32
- Bouton C E et al 2016 Restoring cortical control of functional movement in a human with quadriplegia *Nature* **533** 247–50
- Brandman D M et al 2018 Rapid calibration of an intracortical brain–computer interface for people with tetraplegia *J. Neural. Eng.* **15** 026007
- Brumberg J S, Wright J E, Andreasen DS, Guenther F H and Kennedy P R 2011 Classification of intended phoneme production from chronic intracortical microelectrode recordings in speech-motor cortex *Front. Neurosci.* **5** 65
- Buzsáki G, Anastassiou C A and Koch C 2012 The origin of extracellular fields and currents — EEG, ECoG, LFP and spikes *Nat. Rev. Neurosci.* **13** 407–20
- Chakrabarti S, Sandberg H M, Brumberg J S and Krusienski D J 2015 Progress in speech decoding from the electrocorticogram *Biomed. Eng. Lett.* **5** 10–21
- Chan A M et al 2014 Speech-specific tuning of neurons in human superior temporal gyrus *Cereb. Cortex* **24** 2679–93
- Chang E F and Anumanchipalli G K 2020 Toward a speech neuroprosthesis *JAMA* **323** 413–4

- Chartier J, Anumanchipalli G K, Johnson K and Chang E F 2018 Encoding of articulatory kinematic trajectories in human speech sensorimotor cortex *Neuron* **98** 1042–54.e4
- Chestek C A et al 2011 Long-term stability of neural prosthetic control signals from silicon cortical arrays in rhesus macaque motor cortex *J. Neural. Eng.* **8** 045005
- Cheung C, Hamilton L S, Johnson K and Chang E F 2016 The auditory representation of speech sounds in human motor cortex *eLife* **5** e12577
- Cho K, van Merriënboer B, Gulcehre C, Bahdanau D, Bougares F, Schwenk H and Bengio Y 2014 Learning phrase representations using RNN encoder-decoder for statistical machine translation arXiv: [1406.1078](https://arxiv.org/abs/1406.1078)
- Christie B P, Tat D M, Irwin Z T, Gilja V, Nuyujukian P, Foster J D, Ryu S I, Shenoy K V, Thompson D E and Chestek C A 2015 Comparison of spike sorting and thresholding of voltage waveforms for intracortical brain-machine interface performance *J. Neural. Eng.* **12** 016009
- Collinger J L, Wodlinger B, Downey J E, Wang Wei, Tyler-Kabara E C, Weber D J, McMorland A J C, Velliste M, Boninger M L and Schwartz A B 2013 High-performance neuroprosthetic control by an individual with tetraplegia *Lancet* **381** 557–64
- Coppens P 2016 *Aphasia and Related Neurogenic Communication Disorders* (Burlington, MA: Jones & Bartlett Publishers)
- Creutzfeldt O, Ojemann G and Lettich E 1989 Neuronal activity in the human lateral temporal lobe *Exp. Brain Res.* **77** 451–75
- Dash D, Ferrari P and Wang J 2020 Decoding imagined and spoken phrases from non-invasive neural (MEG) signals *Front. Neurosci.* **14** 290
- Dichter B K, Breshears J D, Leonard M K and Chang E F 2018 The control of vocal pitch in human laryngeal Motor Cortex *Cell* **174** 21–31.e9
- Downey J E, Schwed N, Chase S M, Schwartz A B and Collinger J L 2018a Intracortical recording stability in human brain-computer interface users *J. Neural. Eng.* **15** 046016
- Downey J E, Weiss J M, Fleisher S N, Thumser Z C, Marasco P D, Boninger M L, Gaunt R A and Collinger J L 2018b Implicit grasp force representation in human Motor Cortical recordings *Front. Neurosci.* **12** 801
- Even-Chen N, Stavisky S D, Pandarinath C, Nuyujukian P, Blabe C H, Hochberg L R, Henderson J M and Shenoy K V 2018 Feasibility of automatic error detect-and-undo system in human intracortical brain-computer interfaces *IEEE Trans. Biomed. Eng.* **65** 1771–84
- Guenther F H et al 2009 A wireless brain-machine interface for real-time speech synthesis *PLoS One* **4** e8218
- Heelan C, Lee J, O'Shea R, Lynch L, Brandman D M, Truccolo W and Nurmikko A V 2019 Decoding Speech from Spike-Based Neural Population Recordings in Secondary Auditory Cortex of Non-Human Primates *Commun. Biol.* **2** 1–12
- Herff C D, Heger D, de Pesters A, Telaar D, Brunner P, Schalk G and Schultz T 2015 Brain-to-text: decoding spoken phrases from phone representations in the brain *Front. Neurosci.*
- Herff C, Diener L, Angrick M, Mugler E, Tate M C, Goldrick M A, Krusienski D J, Slutzky M W and Schultz T 2019 Generating natural, intelligible speech from brain activity in motor, premotor, and inferior frontal cortices *Front. Neurosci.* **13**
- Herff C, Krusienski D J and Kubben P 2020 The potential of stereotactic-EEG for brain-computer interfaces: current progress and future directions *Front. Neurosci.* **14** 123
- Herff C and Schultz T 2016 Automatic speech recognition from neural signals: a focused review *Front. Neurosci.* **10** 429
- Hickok G 2012 Computational neuroanatomy of speech production *Nat. Rev. Neurosci.* **13** 135–45
- Hochberg L R et al 2012 Reach and grasp by people with tetraplegia using a neurally controlled robotic arm *Nature* **485** 372–5
- Hochberg L R, Serruya M D, Friehs G M, Mukand J A, Saleh M, Caplan A H, Branner A, Chen D, Penn R D and Donoghue J P 2006 Neuronal ensemble control of prosthetic devices by a human with tetraplegia *Nature* **442** 164–71
- House A S, Williams Carl, Hecker M H L and Kryter K D 1963 Psychoacoustic speech test: a modified rhyme test *PsycEXTRA Dataset*
- Hunt A J and Black A W 1996 Unit selection in a concatenative speech synthesis system using a large speech database 1996 *IEEE Int. Conf. on Acoustics, Speech, and Signal Processing Conf. Proc.* **1** 373–6
- Jarosiewicz B et al 2015 Virtual typing by people with tetraplegia using a self-calibrating intracortical brain-computer interface *Sci. Transl. Med.* **7** 313ra179
- Jiang W, Pailla T, Dichter B, Chang E F and Gilja V 2016 Decoding speech using the timing of neural signal modulation *Conf. Proc. Ann. Int. Conf. IEEE Eng. Med. Biol. Soc.* pp 1532–5
- Kaufman M T, Seely J S, Sussillo D, Ryu S I, Shenoy K V and Churchland M M 2016 The largest response component in the motor cortex reflects movement timing but not movement type *eNeuro* **3** 4
- Kellis S, Miller K, Thomson K, Brown R, House P and Greger B 2010 Decoding spoken words using local field potentials recorded from the cortical surface *J. Neural. Eng.* **7** 056007
- Kingma D P and Ba J 2017 Adam: A method for stochastic optimization arXiv: [1412.6980](https://arxiv.org/abs/1412.6980)
- Kobak D, Brendel W, Constantinidis C, Feierstein C E, Kepecs A, Mainen Z F, Qi X L, Romo R, Uchida N and Machens C K 2016 Demixed principal component analysis of neural population data *eLife* **5** e10989
- Koch S, Fried-Oken M, Jakobs T and Beukelman D R 2019 New and emerging access technologies for adults with complex communication needs and severe motor impairments: state of the science *Augmentative Altern. Commun.* **35** 13–25
- Li L and Negoita S 2018 Brain-to-speech decoding will require linguistic and pragmatic data *J. Neural. Eng.* **15** 063001
- Lipski W J et al 2018 Subthalamic nucleus neurons differentially encode early and late aspects of speech production *J. Neurosci.* **38** 5620–31
- Livezey J A, Bouchard K E and Chang E F 2019 Deep learning as a tool for neural data analysis: speech classification and cross-frequency coupling in human sensorimotor cortex *PLoS Comput. Biol.* **15** e1007091
- Lotte F, Brumberg J S, Brunner P, Gunduz A, Ritaccio A L, Guan C and Schalk G 2015 Electrographic representations of segmental features in continuous speech *Front. Hum. Neurosci.* **9** 97
- Makin J G, Moses D A and Chang E F 2020 Machine translation of cortical activity to text with an encoder-decoder framework *Nat. Neurosci.* **23** 575–82
- Makonen T, Ruottinen H, Puhto R, Helminen M and Palmio J 2018 Speech deterioration in amyotrophic lateral sclerosis (ALS) after manifestation of bulbar symptoms *Int. J. Lang. Commun. Disord. R. Coll. Speech Lang. Ther.* **53** 385–92
- Martin S, Brunner P, Holdgraf C, Heinze H-J, Crone N E, Rieger J, Schalk G, Knight R T and Pasley B N 2014 decoding spectrotemporal features of overt and covert speech from the human cortex *Front. Neuroeng.* **7** 14
- Martin S, Iturrate I, Millán J D R, Knight R T and Pasley B N 2018 Decoding inner speech using electrocorticography: progress and challenges toward a speech prosthesis *Front. Neurosci.* **12** 422
- Mcfee B et al 2019 *Librosa/librosa: 0.7. 1 Version 0. 7 1*
- Mines M A, Hanson B F and Shoup J E 1978 Frequency of occurrence of phonemes in conversational English *Lang. Speech* **21** 221–41
- Moses D A, Leonard M K, Makin J G and Chang E F 2019 Real-time decoding of question-and-answer speech dialogue using human cortical activity *Nat. Commun.* **10** 1–14
- Mugler E M, Patton J L, Flint R D, Wright Z A, Schuele S U, Rosenow J, Shih J J, Krusienski D J and Slutzky M W 2014 Direct classification of all American English phonemes using signals from functional speech motor cortex *J. Neural. Eng.* **11** 035015

- Mugler E M, Tate M C, Livescu K, Templer J W, Goldrick M A and Slutzky M W 2018 Differential representation of articulatory gestures and phonemes in precentral and inferior frontal gyri *J. Neurosci.* **38** 9803–13
- Nason S R et al 2020 Low-power 'spiking band' feature is dominated by local single units and improves brain-machine interface performance *Nat. Biomed. Eng.* **4** 973–83
- Nguyen C H, Karavas G K and Artemiadis P 2018 Inferring imagined speech using EEG signals: a new approach using Riemannian manifold features *J. Neural. Eng.* **15** 016002
- O'Shea D J and Shenoy K V 2018 ERAASR: an algorithm for removing electrical stimulation artifacts from multielectrode array recordings *J. Neural. Eng.* **15** 026020
- Oby E R, Perel S, Sadtler P T, Ruff D A, Mischel J L, Montez D F, Cohen M R, Batista A P and Chase S M 2016 Extracellular voltage threshold settings can be tuned for optimal encoding of movement and stimulus parameters *J. Neural. Eng.* **13** 036009
- Pailla T, Jiang W, Dichter B, Chang E F and Gilja V 2016 ECoG data analyses to inform closed-loop BCI experiments for speech-based prosthetic applications *Ann. Int. Conf. IEEE Eng. Med. Biol. Soc.* pp 5713–6
- Pandarinath C, Nuyujukian P, Blabe C H, Sorice B L, Saab J, Willett F R, Hochberg L R, Shenoy K V and Henderson J M 2017 High performance communication by people with paralysis using an intracortical brain-computer interface *eLife* **6** e18554
- Pedregosa F et al 2011 Scikit-learn: machine learning in python *J. Mach. Learn. Res.* **12** 2825–30
- Perge J A, Homer M L, Malik W Q, Cash S, Eskandar E, Friehs G, Donoghue J P and Hochberg L R 2013 Intra-day signal instabilities affect decoding performance in an intracortical neural interface system *J. Neural. Eng.* **10** 036004
- Rabbani Q, Milsap G and Crone N E 2019 The potential for a speech brain-computer interface using chronic electrocorticography *Neurother.J. Am. Soc. Exp. Neuro. Ther.* **16** 144–65
- Ramsey N F, Salari E, Aarnoutse E J, Vansteensel M J, Bleichner M G and Freudenburg Z V 2018 Decoding spoken phonemes from sensorimotor cortex with high-density ECoG grids *NeuroImage* **180** 301–11
- Rastogi A et al 2020 Neural representation of observed, imagined, and attempted grasping force in Motor Cortex of individuals with chronic tetraplegia *Sci. Rep.* **10** 1429
- Roussel P et al 2020 Observation and assessment of acoustic contamination of electrophysiological brain signals during speech production and sound perception *J. Neural. Eng.*
- Salari E, Freudenburg Z V, Vansteensel M J and Ramsey N F 2018 The influence of prior pronunciations on sensorimotor cortex activity patterns during vowel production *J. Neural. Eng.* **15** 066025
- Slutzky M W 2019 Brain-machine interfaces: powerful tools for clinical treatment and neuroscientific investigations *Neurosci. A* **25** 139–54
- Sokal R R and Michener C D 1958 A statistical method for evaluating systematic relationships *University of Kansas Science Bulletin* (Lawrence, KS: University of Kansas) **28** 1409–38
- Stark E and Abeles M 2007 Predicting movement from multiunit activity *J. Neurosci.* **27** 8387–94
- Stavisky S D et al 2019 Neural ensemble dynamics in dorsal motor cortex during speech in people with paralysis *eLife* **8** e46015
- Stavisky S D, Rezaei P, Willett F R, Hochberg L R, Shenoy K V and Henderson J M 2018 Decoding speech from intracortical multielectrode arrays in dorsal 'arm/hand areas' of human Motor Cortex 2018 40th Annual Int. Conf. of the IEEE Eng. Med. Biol. Soc. (EMBC) 93–97
- Stavisky S D, Willett F R, Avansino D T, Hochberg L R, Shenoy K V and Henderson J M 2020 Speech-related dorsal motor cortex activity does not interfere with iBCI cursor control *J. Neural. Eng.* **17** 016049
- Stevens S S, Volkman J and Newman E B 1937 A scale for the measurement of the psychological magnitude pitch *J. Acoust. Soc. Am.* **8** 185–90
- Suppes P, Lu Z L and Han B 1997 Brain wave recognition of words *Proc. Natl Acad. Sci. USA* **94** 14965–9
- Sussillo D, Stavisky S D, Kao J C, Ryu S I and Shenoy K V 2016 Making brain-machine interfaces robust to future neural variability *Nat. Commun.* **7** 1–13
- Tai K, Blain S and Chau T 2008 A review of emerging access technologies for individuals with severe motor impairments *Assist. Technol.* **20** 204–19; 220–21
- Takai O, Brown S and Liotti M 2010 Representation of the speech effectors in the human motor cortex: somatotopy or overlap? *Brain Lang.* **113** 39–44
- Tam W-K, Wu T, Zhao Q, Keefer E and Yang Z 2019 Human motor decoding from neural signals: a review *BMC Biomed. Eng.* **1** 22
- Tankus A and Fried I 2019 Degradation of neuronal encoding of speech in the subthalamic nucleus in Parkinson's disease *Neurosurgery* **84** 378–87
- Tankus A, Fried I and Shoham S 2012 Structured neuronal encoding and decoding of human speech features *Nat. Commun.* **3** 1–5
- Tourville J A and Guenther F H 2011 The DIVA model: a neural theory of speech acquisition and production *Lang. Cogn. Process.* **26** 952–81
- Trautmann E M et al 2019 Accurate estimation of neural population dynamics without spike sorting *Neuron* **103** 292–308.e4
- Waldert S, Lemon R N and Kraskov A 2013 Influence of spiking activity on cortical local field potentials *J. Physiol.* **591** 5291–303
- Willett F R, Avansino D, Hochberg L, Henderson J and Shenoy K 2020a High-performance brain-to-text communication via imagined handwriting (accepted) (<https://doi.org/10.1101/2020.07.01.183384>)
- Willett F R, Deo D R, Avansino D T, Rezaei P, Hochberg L R, Henderson J M and Shenoy K V 2020b Hand knob area of premotor cortex represents the whole body in a compositional way *Cell* **181** 396–409.e26
- Wodlinger B, Downey J E, Tyler-Kabara E C, Schwartz A B, Boninger M L and Collinger J L 2015 Ten-dimensional anthropomorphic arm control in a human brain-machine interface: difficulties solutions, and limitations *J. Neural Eng.* **12** 20
- Young D, Willett F, Memberg W D, Murphy B, Walter B, Sweet J, Miller J, Hochberg L R, Kirsch R F and Ajiboye A B 2018 Signal processing methods for reducing artifacts in microelectrode brain recordings caused by functional electrical stimulation *J. Neural. Eng.* **15** 026014
- Zhang M et al 2018 Extracting wavelet based neural features from human intracortical recordings for neuroprosthetics applications *Bioelectron. Med.* **4** 11